THE ROTARY MOTOR OF BACTERIAL FLAGELLA

Howard C. Berg

Department of Molecular and Cellular Biology, Harvard University, 16 Divinity Avenue, Cambridge, Massachusetts 02138; email: hberg@biosun.harvard.edu

Key Words   *Escherichia coli*, motility, chemotaxis, ion flux, torque generation

■ **Abstract**   Flagellated bacteria, such as *Escherichia coli*, swim by rotating thin helical filaments, each driven at its base by a reversible rotary motor, powered by an ion flux. A motor is about 45 nm in diameter and is assembled from about 20 different kinds of parts. It develops maximum torque at stall but can spin several hundred Hz. Its direction of rotation is controlled by a sensory system that enables cells to accumulate in regions deemed more favorable. We know a great deal about motor structure, genetics, assembly, and function, but we do not really understand how it works. We need more crystal structures. All of this is reviewed, but the emphasis is on function.

CONTENTS

INTRODUCTION

The bacterial flagellar motor is a nanotechnological marvel, no more than 50 nm in diameter, built from about 20 different kinds of parts. It spins clockwise (CW) or counterclockwise (CCW) at speeds on the order of 100 Hz, driving long thin helical

filaments that enable cells to swim. Peritrichously flagellated cells (*peri,* around; *trichos*, hair), such as *Escherichia coli*, execute a random search, moving steadily at about 30 diameters per second, now in one direction, now in another. Steady motion requires CCW rotation. Receptors near the surface of the cell count molecules of interest (sugars, amino acids, dipeptides) and control the direction of flagellar rotation. If a leg of the search is deemed favorable, it is extended, i.e., the motors spin CCW longer than they otherwise would. This bias enables cells to actively find regions in their environment where life is better. Thus, the flagellar motor is the output organelle of a remarkable sensory system, the components of which have been honed to perfection by billions of years of evolution.

We know a great deal about the structure of the flagellar motor but not very much at atomic resolution. We know a great deal about regulation of the genes that specify the motor's component parts and how those parts are assembled. We know a great deal about motor function: about the fuel that powers the motor, the torque that it can generate at different speeds, and what controls the likelihood that it changes direction. However, we do not know how the motor actually works, i.e., the details of what makes it go, or how it manages to shift abruptly from forward (CCW) to reverse (CW).

The work described here has been done primarily with the gram-negative organisms, *E. coli* and *Salmonella enterica* serovar Typhimurium (*Salmonella* for short), that are closely related. Their motors are driven by protons powered by a transmembrane electrochemical gradient, or protonmotive force. ATP plays no role, except in motor assembly and in chemotactic signaling (coupling of receptors and flagella). However, if cells are grown anaerobically, ATP generated by glycolysis powers a membrane H^+-ATPase that maintains the protonmotive force. A gram-positive *Streptococcus* has been useful for studies of membrane energetics. Gram-negative marine *Vibrio* spp. have motors that are driven by sodium ions rather than protons, and comparisons between different kinds of ion-driven machines are illuminating. Flagellar motors are important in a wide variety of other bacteria, from *Caulobacter* to *Leptospira*, not considered here.

In this chapter I review what is known about motor structure, genetics, and assembly, say more about function, and then touch upon motor mechanisms.

STRUCTURE

E. coli is rod-shaped, about 1 μm in diameter by 2 μm long. A cell is propelled by a set of four helical flagellar filaments (four, on average) that arise at random points on its sides and extend several body lengths out into the external medium. Each filament is driven at its base by a rotary motor embedded in the cell envelope. A cell swims steadily in a direction roughly parallel to its long axis for about a second—it is said to "run"—and then moves erratically in place for a small fraction of a second—it is said to "tumble"—and then swims steadily again in a new direction. When a cell runs at top speed, all of its flagellar filaments spin

CCW (as viewed along a filament from its distal end toward the cell body); the filaments form a bundle that pushes the cell steadily forward. When a cell tumbles, one or more filaments spin CW (1–3); these filaments leave the bundle, and the cell changes course (see below). Motors switch from CCW to CW and back again approximately at random. The likelihood of spinning CW is enhanced by a chemotactic signaling protein, CheY. When phosphorylated, CheY binds to the cytoplasmic face of the flagellar motor. The phosphorylation of CheY is catalyzed by a kinase, the activity of which is controlled by chemoreceptors. The activity of the kinase is depressed by the addition of attractant. (For recent reviews on bacterial chemotaxis, see References 4–11.)

A bacterial flagellum is shown schematically in Figure 1, along with a reconstruction of the motor core obtained by rotationally averaging images taken by electron microscopy. A gram-negative bacterium has a multilayered cell envelope. Note the positions of the inner (cytoplasmic) membrane, the peptidoglycan layer, and the outer membrane. The different components of the motor are named after the genes that encode them. A parts list is given in Table 1.

Originally, genes for which mutant cells lacked flagellar filaments were called *fla* (for flagellum), but after more than 26 had been found and the correspondence between genes in *E. coli* and *Salmonella* became clear, the nomenclature was simplified (12); *fla* genes are now called *flg, flh, fli,* or *flj,* depending upon their location on the genetic map. Genes for which mutant cells produce paralyzed flagella are called *mot* (for motility). Four of the 40 gene products listed in the table are involved in gene regulation (FlgM, FlhC, FlhD, FliA); see below. About half appear in the final structure (Figure 1). The hook (FlgE), the hook-associated proteins (FlgK, FlgL, and FliD), and the filament (FliC) are outside the cell; the MS-ring (FliF) and the P- and L-rings (FlgI and FlgH) are embedded in the cell wall; and the C-ring (FliM and FliN) is inside the cell. FliG is bound to the inner face of the MS-ring near its periphery. In some reports, it is treated as part of the C-ring. MotA and MotB, which are arranged in a circular array around the MS- and C-rings, span the inner membrane.

The hook and filament are polymers (crystals) of single polypeptides, hook protein (FlgE) and flagellin (FliC), respectively. They comprise 11 parallel rows of subunits on the surface of a cylinder, with the rows tilted (twisted) slightly relative to the local cylinder axis, as shown in Figure 2. The subunits pack in two different ways: The subunits in "short" protofilaments (R-type) are closer together than the subunits in "long" protofilaments (L-type). R and L refer to the direction of twist. If both types are present at the same time, the filament has curvature as well as twist and is helical, with the short protofilaments running along the inside of the helix (13). Mechanical strain energy is minimized when short protofilaments are next to short protofilaments and long protofilaments are next to long protofilaments, leading to 12 possible conformations, 2 straight (all short or all long) and 10 helical (14, 15).

The hook is flexible. As it rotates, its protofilaments continuously switch from short to long, so that short protofilaments always appear at the inside of the bend.
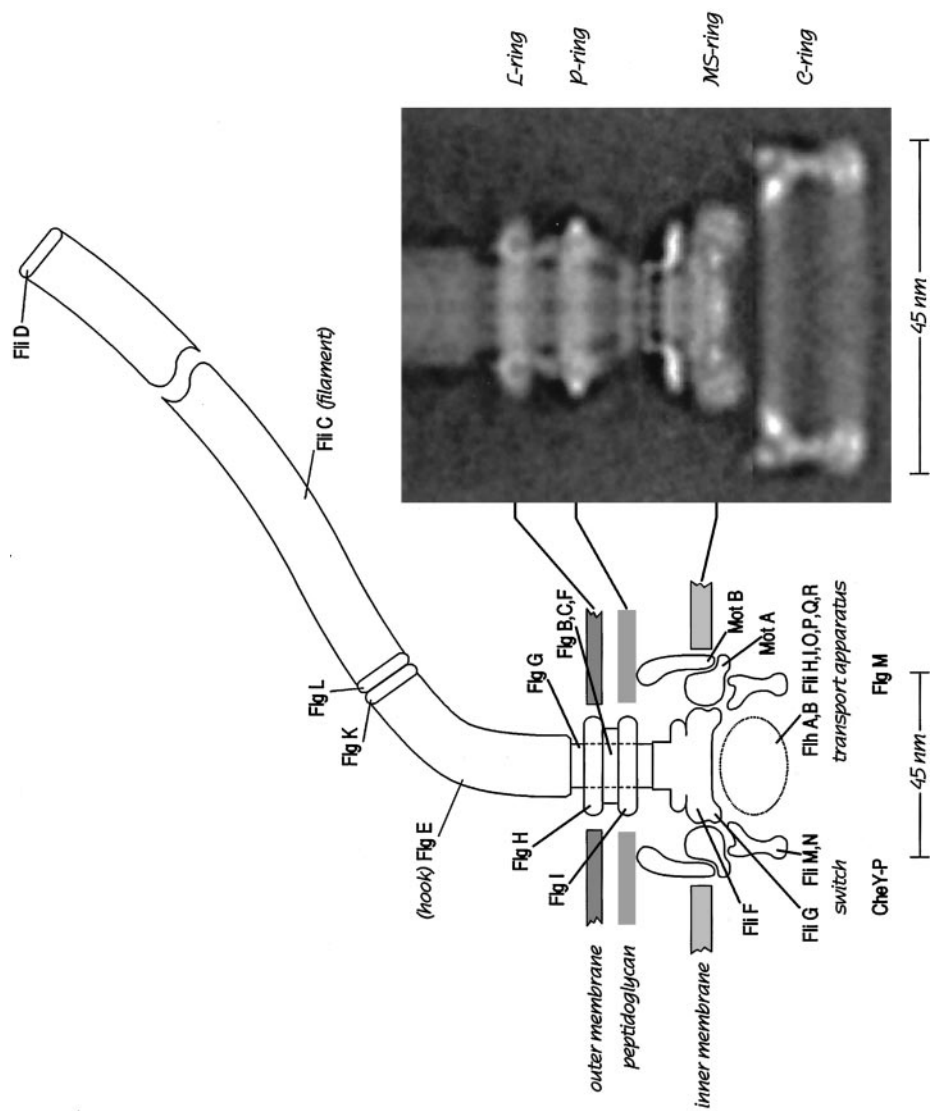
The filament, on the other hand, is rigid, with a shape that depends on the amino acid sequence of the flagellin, the pH, ionic strength, and torsional load. When one or more motors on the cell switch from CCW to CW, their filaments go through a sequence of transformations, from normal to semicoiled to curly 1; when the motors switch back to CCW, they revert to normal, as shown in Figure 3. The normal filament, with 2 short protofilaments, is left-handed. The semi-coiled filament, with 4, is right-handed with half the normal pitch. The curly 1 filament, with 5, is right-handed with half the normal pitch and half the normal amplitude. Evidently, the hook-associated proteins FlgK and FlgL (Figure 1) allow the protofilaments of the hook to switch from short to long but require that the protofilaments of the filament remain fixed. There are mutants of *flgL* that allow filaments to switch from normal to straight or from curly 1 to straight, depending upon the direction of rotation of the flagellar motor (16). These transformations are forbidden in the wild type. So, the response of the filament to torsion depends, in part, on how it is held at its base. (For recent discussions of filament structure, see References 17–19.) A flagellin truncated at both its N and C termini (to block filament formation) has been crystallized, and the transformation responsible for the switch from "short" to "long" has been identified by computer simulation (20).

Early on, it was thought that the basal body (the structure proximal to the hook) comprises four rings (M, S, P and L) and a rod, because these elements could be seen by electron microscopy when flagella were purified and negatively stained. In this procedure, cell walls were weakened by treatment with EDTA and lysozyme, cells were lysed with a nonionic detergent and treated with DNase I, and flagella were fractionated in detergent by differential sedimentation (21). The rings were named by DePamphilis & Adler (22), who found that the M-ring (for membrane) has affinity for inner-membrane fractions, the S-ring (for supramembranous) is seen just above the inner membrane, the P-ring (for

←

Figure 1 A schematic diagram of the flagellar motor, drawn to scale, compared to a rotationally averaged reconstruction of images of hook-basal bodies seen in an electron microscope. The different proteins are named for their genes and are listed in Table 1. CheY-P is the chemotaxis signaling molecule that binds to FliM, and FlgM is the anti-sigma factor pumped out of the cell by the transport apparatus; see the text. The general morphological features are C-ring, MS-ring, P-ring, L-ring, hook, hook-associated proteins (which include the distal cap), and filament. MotA, MotB, and components of the transport apparatus (dashed ellipse) do not survive extraction with detergent and, therefore, are not shown on the right. This reconstruction is derived from rotationally averaged images of about 100 hook–basal body complexes of *Salmonella* polyhook strain SJW880 embedded in vitreous ice (29). The radial densities have been projected from front to back along the line of view, so this is what would be seen if one were able to look through the spinning structure. Connections between the C-ring and the rest of the structure appear relatively tenuous. Digital print courtesy of D.J. DeRosier.

TABLE 1 Proteins of *E. coli* involved in flagellar motor assembly and function[a]

Gene product	Function or motor component	Size (kDa)	Copies per motor[b]	Operon class[c]
FlgA	Assembly of P-ring	24		2
FlgB	Proximal rod	15	6	2
FlgC	Proximal rod	14	6	2
FlgD	Assembly of hook	24		2
FlgE	Hook	42	130	2
FlgF	Proximal rod	26	6	2
FlgG	Distal rod	28	26	2
FlgH	L-ring	22	26	2
FlgI	P-ring	36	26	2
FlgJ	Muramidase	34		2
FlgK	Hook-filament junction; at hook	59	11	3a
FlgL	Hook-filament junction; at filament	34	11	3a
FlgM	Anti-sigma factor	11		3a
FlgN	FlgK, FlgL chaperone	16		3a
FlhA	Protein export	75		2
FlhB	Hook-length control	42		2
FlhC	Master regulator for class 2 operons	22		1
FlhD	Master regulator for class 2 operons	14		1
FlhE	?	12		2
FliA	Sigma factor for class 3 operons	27		2
FliC	Filament (flagellin)	55	5340	3b
FliD	Filament cap	50	10	3a
FliE	Rod MS-ring junction (?)	11	9?	2
FliF	MS-ring	61	26	2
FliG	Rotor component; binds MotA	37	26	2
FliH	Protein export	26		2
FliI	Protein export ATPase	49		2
FliJ	Rod, hook, filament chaperone	17		2
FliK	Hook-length control	39		2
FliL	?	17		2
FliM	Switch component; binds CheY-P	38	32?	2
FliN	Switch component	14	110	2
FliO	Protein export	11		2

TABLE 1 Continued

Gene product	Function or motor component	Size (kDa)	Copies per motor[b]	Operon class[c]
FliP	Protein export	27		2
FliQ	Protein export	10		2
FliR	Protein export	29		2
FliS	FliC chaperone	15		3a
FliT	FliD chaperone	14		3a
MotA	Force-generator	32	32?	3b
MotB	Force-generator	34	16?	3b

[a]Including proteins involved in gene regulation but not in signal processing. *flg* genes are in map region I (*E. coli* 24 min, *Salmonella* 23 min); *flh* and *mot* genes are in map region II (41 min, 40 min); and *fli* genes are in map region III (43 min, 40 min). For operons, additional gene products in *Salmonella*, and references to gene sequences, see Table 1 of Macnab (246).

[b]Approximate values. The figure given for FliC (flagellin) is subunits per turn of the normal helix (17).

[c]Class 3 operons that have some FliA-independent expression are designated 3a and those that do not, 3b (254, 258).

peptidoglycan) is at the right place to be embedded in the peptidoglycan, and the L-ring (for lipopolysaccharide) has affinity for outer-membrane fractions (23).

In the earliest models for the rotary motor (24), the M-ring was thought to rotate relative to the S-ring, which served as the stator. Later it was found that both the M- and S-rings (now called the MS-ring) comprise different domains of the same protein, FliF (25, 26). Therefore, they function as a unit. The C-ring (for cytoplasmic) was discovered much later when extracts were treated more gently, i.e., subjected to smaller extremes of pH and ionic strength (27–29). The image shown in Figure 1 was reconstructed from basal bodies prepared gently and examined in frozen-hydrated preparations in a cryoelectron microscope. Freeze-etch replicas made in situ show a knob in the center of each C-ring; the knob is thought to comprise the main body of the transport apparatus (30; see also Reference 31).

FliG, FliM, and FliN are also referred to as the "switch complex," since many mutations of *fliG, fliM,* and *fliN* lead to defects in switching (in control of the direction of rotation) (32, 33). Other mutations are nonmotile, and the null phenotypes are nonflagellate. The chemotactic signaling protein, CheY-P, binds to FliM (34–37). A variety of binding studies argue that FliG binds to FliF (38, 39) and FliG, FliM, and FliN bind to each other (36, 39, 40). Functional or partially functional in-frame fusions have been obtained between FliF and FliG (41, 42) and between FliM and FliN (43), but not between FliG and FliM (44). Fusions of the latter type block flagellar assembly. An electron micrographic analysis of basal-body structures found in nonmotile missense mutations of *fliG, fliM,* and *fliN* indicates loss of the C-ring, the components of which (FliM and
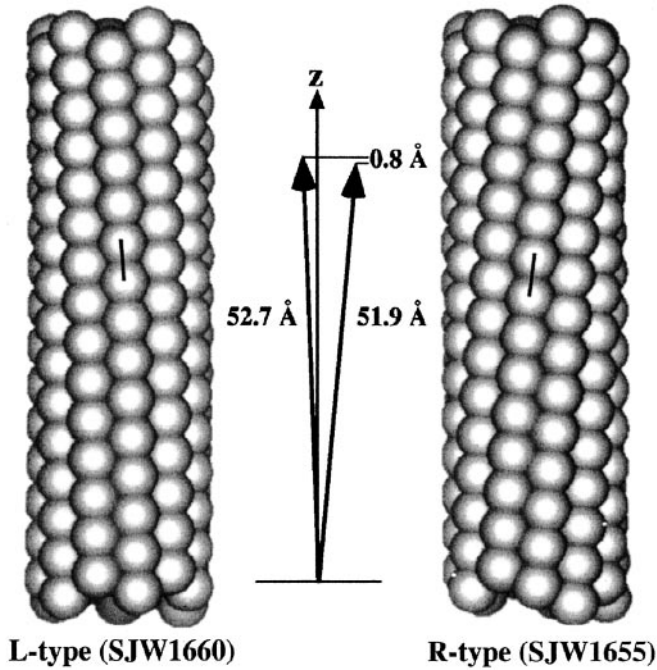
Figure 2 The surface lattice of L- and R-type straight flagellar filaments. The spacing between flagellin subunits along an 11-start helix (a protofilament) of the R-type is 0.07 nm less than between corresponding subunits of the L-type. L and R refer to the handedness of the filament twist. The SJW numbers designate particular bacterial strains. The distances are measured at a radius of 4.5 nm and are shown magnified in the middle of the drawing. (From Reference 19, Figure 19.)

FliN) can be recovered in the cytoplasm (45, 46). And nonmotile mutations of *fliM* and *fliN,* but not *fliG,* can be cured by overexpression (47). So attachment of the C-ring appears to be labile, as suggested by the region of low density between this structure and the rest of the basal body evident in the image reconstruction of Figure 1. Although it is conceivable that these structures rotate relative to one another (48), most workers assume that they rotate as a unit, i.e., that the rotor comprises both the MS- and C-rings.

The stator is thought to comprise the MotA and MotB proteins, which are membrane embedded and do not fractionate with the rest of the hook–basal body complex (49). However, they can be visualized as circular arrays of membrane particles ("studs") in freeze-fracture preparations of the inner membrane. Studs were seen first at the poles of *Aquaspirillum serpens* in sets of 14–16 (50), later in *Streptococcus* in similar numbers and in *E. coli* in sets of 10–12 (51), and finally in *Salmonella* and different species of *Bacillus* in sets of about 12 (52, 53).
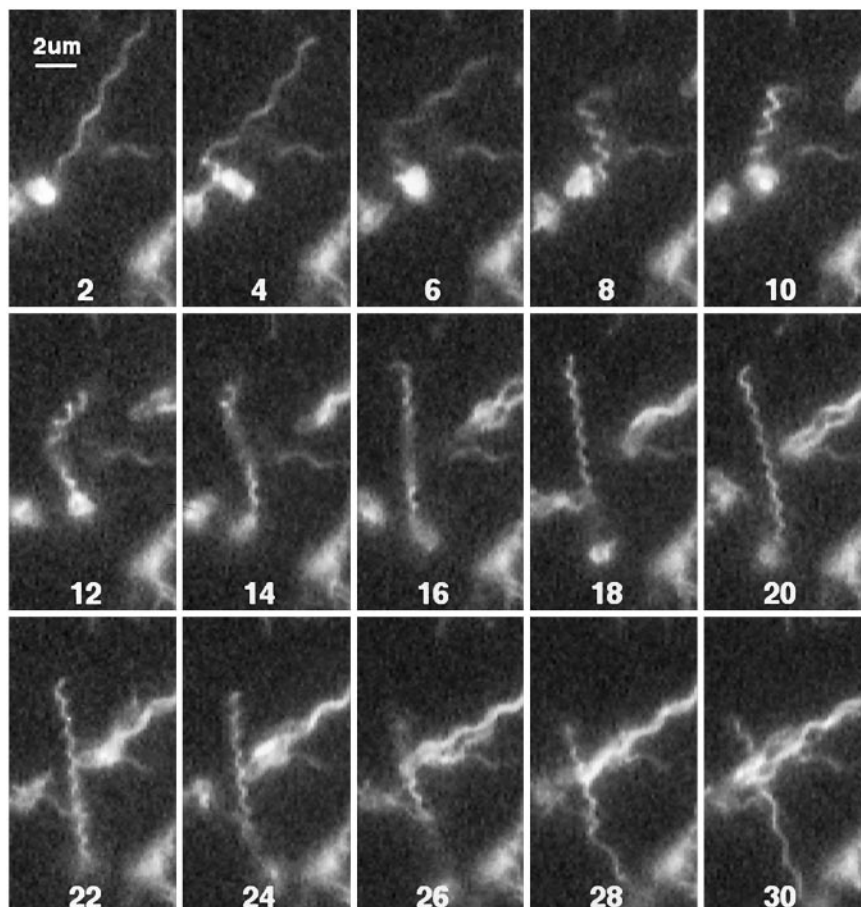
Figure 3   An *E. coli* cell with one flagellar filament, visualized by fluorescence microscopy. The recording was made at 60 Hz, but only every other field is shown. The numbers are in units of 1/60 s. When the motor switched from CCW to CW after field 2, the filament changed its shape from normal to semicoiled, 10, and then to curly 1, e.g., 20. When the motor switched back to CCW after field 26, the filament relaxed back to normal, 30. Initially, the cell swam toward 7 o'clock. After the normal to semicoiled transformation, it swam toward 5 o'clock. Flagellar filaments can also be visualized by dark-field or interference-contrast microscopy (259, 260), but fluorescence has the advantage that one can see the filaments all the way to the surface of the cell with reasonable depth of field. (From Reference 3, Figure 6.)

Both MotA and MotB span the cytoplasmic membrane. MotA has four membrane-spanning α-helical segments (54–56). The rest of the molecule (about two-thirds) is in the cytoplasm. MotB has one membrane-spanning α-helical

segment near its N terminus, but most of the molecule is in the periplasmic space (57, 58). There is a peptidoglycan-binding domain near its C terminus (59) (although such binding has not been shown directly). MotB is thought to anchor MotA to the rigid framework of the cell wall. Elements of the stator must be anchored to this framework somewhere, or torque cannot be delivered to the flagellar filament (24). Evidently, MotA and MotB form a complex that acts as a torque-generating unit. The stoichiometry of each unit is not known for certain, but it is likely to be four MotA and two MotB. This arrangement is suggested from reconstitution of the *Vibrio* homologs, PomA and PomB (60). MotA and MotB can be co-isolated by an affinity tag on MotB, and thus these proteins bind to each other (40). Targeted disulfide cross-linking of the transmembrane segment of MotB indicates a symmetric arrangement of parallel α-helices (61), suggesting that each torque-generating unit contains at least two copies of MotB. Earlier, tryptophan-scanning mutagenesis had suggested a model in which the transmembrane segment of one MotB is bundled slantwise with the four transmembrane segments of one MotA to constitute a proton channel (62, 63). It appears likely, now, that there are two proton channels per complex, each comprising eight transmembrane segments from two copies of MotA and one transmembrane segment from one copy of MotB (61).

Studies of extragenic suppression of dominant missense mutations of *motA* (64) and *motB* (65, 66) suggest that MotA and MotB interact with FliG (a component at the cytoplasmic face of the MS-ring; see Figure 1) as well as with each other. Mutations near the putative peptidoglycan-binding region of MotB appear to misalign the stator and the rotor (66). Comparison of residues conserved in different bacterial species and site-directed mutagenesis have identified charged groups in the cytoplasmic domain of MotA that interact with other charged groups (primarily of opposite sign) in the C-terminal domain of FliG (67–69). Similar studies have implicated a particular aspartate residue of MotB (Asp32), located at the cytoplasmic end of the membrane channel, as a proton acceptor (70). Two proline residues in MotA (Pro173 and Pro222), also located at the cytoplasmic end of this channel, have been shown to be important for function (67, 71). Mutations in either Asp32 or Pro173 in membrane-bound complexes of MotA and MotB alter the susceptibility of MotA to proteolysis, providing additional evidence for changes in its conformation (72). Thus, it appears that torque is generated as protonation and deprotonation of Asp32 of MotB modulates the conformation of MotA, changing the interaction of a specific charged region in the cytoplasmic domain of MotA with a complementary charged region in the C-terminal domain of FliG. To see how this might happen, we need crystal structures of MotA, MotB, and FliG. Crystal structures of the C-terminal and middle domains of FliG have been obtained from the hyperthermophylic eubacterium, *Thermotoga maritima* (73, 74). These structures suggest that the charged groups implicated by site-directed mutagenesis might, indeed, be arrayed on the periphery of the rotor. To understand torque generation,

TABLE 2 Operons encoding the proteins of the chemotaxis system of *E. coli*[a]

Class 1	Class 2	Class 3
flhDC	*flgAMN*	*fliC*
	flgBCDEFGHIJKL	*motABcheAW*
	flhBAE	*tar tap cheRBYZ*
	fliAZY	*aer*
	fliDST	*trg*
	fliE	*tsr*
	fliFGHIJK	
	fliLMNOPQR	

[a]The underlined genes belong to the operons shown, activated by FlhDC, but they have additional promoters activated by FliA. Thus, they are expressed partially as class 2 genes and fully as class 3 genes. Class 3 genes not mentioned in the early part of the text encode receptors for aspartate (*tar*), dipeptides (*tap*), ribose and galactose (*trg*), and serine (*tsr*), a sensor for redox potential (*aer*), enzymes involved in sensory adaptation, a methyltransferase (*cheR*) and methylesterase (*cheB*), and an enzyme that accelerates the removal of phosphate from CheY-P (*cheZ*).

however, we need to know how the complementary groups on MotA interact with these sites and how these interactions change during proton translocation.

GENETICS

Genes expressing flagellar components are arranged in hierarchical order (75, 76) in three classes, as shown in Table 2. Class 1 contains the master operon, *flhDC,* the expression of which is required for transcription of class 2 and class 3 operons (77). Class 2 contains eight operons that encode components required for construction of the hook-basal body complex, and class 3 contains six more that encode components required for filament assembly and motor function. If nutrients are plentiful, motility and chemotaxis are considered luxuries, and cells dispense with them; for example, when *E. coli* is grown on glucose, flagellar synthesis is suppressed (78). *flhDC* is subject to activation by the catabolite repressor/activator protein (CAP) and cyclic AMP (79). It also is activated by the histone-like protein H-NS (80). Also, *flhDC* stimulates *fliA* expression; and *fliA*, in turn, further stimulates *flhDC* expression, which provides a self-reinforcing feedback loop to ensure expression of flagellar genes when needed (81) (see below). Connections between *flhDC* and other systems exist, e.g., those mediating response to heat shock (82), controlling cell division (83), or regulating synthesis of type 1 pili (84). These are not discussed further here (for a short review, see Reference 85). However, one dramatic example of flagellar up-

regulation that should be mentioned is swarming, in which cells lengthen, produce large numbers of flagella, and spread rapidly over the surface of hard agar (86, 87). The chemotaxis system itself, which requires expression of *flhDC*, appears to be involved in this process (88).

FliA, the gene product of a class 2 operon, is the sigma factor for transcription of class 3 operons (89). FlgM is an anti-sigma factor, i.e., an anti-FliA (90–92). FlgM is encoded by a class 3 gene, but it can also be expressed by readthrough from the class 2 *flgA* promoter (93, 94). Upon completion of the hook–basal body complex, just before the hook-associated proteins are added, the motor transport apparatus pumps FlgM out of the cell (94, 95). As a result, class 3 genes are activated. FlgM is a small protein (97 amino acids) that is largely unfolded, and its conformational plasticity is thought to expedite export (96). The removal of this protein allows cells to finish construction of the machinery needed for motility and chemotaxis. The economy here is that cells do not waste energy synthesizing the large amount of flagellin required for flagellar filaments unless rotary motors are assembled and ready to put these filaments to use. Nor do cells synthesize the torque-generating units MotA and Mot B, or components of the chemotaxis system, such as CheY unless hook and basal body assembly has been successful. The hook-associated proteins are encoded by class 3 operons, but they also are expressed at low levels in the absence of FliA, so the hook–basal body complex can be completed prior to the synthesis of flagellin (97, 98). In short, flagellar genes are expressed in the order in which their products are needed for assembly (99, 100).

ASSEMBLY

The motor is built from the inside out (for minireviews, see References 101, 102). This order was recognized by Suzuki et al. (103), who studied mutants of *Salmonella* defective for different *fla* genes and searched in pellets obtained from detergent extracts for incomplete flagellar structures. The simplest structure found was a "rivet," comprising the MS-ring and rod. Similar results were obtained with mutants of *E. coli* (104). A more recent study identified an even simpler initial structure, the MS-ring alone, and provided many details of the morphological pathway (105). FliG and the C-ring (FliM and FliN) are added to the MS-ring (FliF); see Figure 1. No other proteins are required for this construction (106). Then the transport apparatus is assembled (FlhA, FlhB, FliH, FliI, FliO, FliP, FliQ, FliR) (see References 107–113). This apparatus is used to pass components for other axial structures through a channel at the center of the MS-ring.

One of the key components of the transport apparatus, FliI, shows homology to both the β subunit of the F_0F_1-ATPase (107) and to components of bacterial type III secretory systems (114). Purified His-tagged FliI binds and hydrolyzes

ATP (115). FliI is inhibited by FliH, a component thought to ensure that hydrolysis is properly linked to transport of exported substrates (116).

In *Salmonella,* the type III secretion system injects virulence factors into epithelial cells of the small intestine, inducing them to engulf bacteria. This injection has been shown to involve needle structures, having components homologous to those of the transport apparatus of the flagellar motor (117, 118; for a general review, see Reference 119).

Cytoplasmic chaperones (Table 1) aid in the transport process, in part by preventing aggregation (120–125; for reviews, see References 126, 127).

The next components to be added include the proximal (FlgB, FlgC, FlgF) and distal rod (FlgG) (128). FliE is needed for this assembly and is thought to form a junction between the MS ring and the proximal part of the rod (129, 130). Construction of the hook (FlgE) begins, but it does not proceed very far until the P- and L-rings (FlgI and FlgH) are assembled. Components for these structures are secreted into the periplasmic space by the signal-peptide-dependent (Sec) secretory machinery (131, 132). Assembly of the P-ring also requires FlgA (133), as well as formation of disulfide bonds catalyzed by DsbA and DsbB (134). Formation of the L-ring requires the activity of a flagellum-specific muramidase, FlgJ, that also plays a role in rod formation (135). The L-ring constituent, FlgH, is a lipoprotein (136).

The hook is assembled with the aid of a cap at its distal end (FlgD), which is then discarded (137). Hook length, normally ∼55 nm (138), is determined to a precision of about 10%, but the mechanism for this length control is not known. The key player is a cytoplasmic protein called FliK. If this protein is missing, cells form long hooks, called polyhooks (139, 140). However, some control remains, because the distribution of polyhook lengths still peaks at ∼55 nm (141). If FliK were simply a molecular ruler, truncated FliK proteins should form shorter hooks, but all *fliK* mutants studied thus far produce longer hooks (142). FliK is exported during hook assembly, and export-deficient *fliK* mutants also produce long hooks (143). Normally, cellular levels of hook protein do not matter, but if FliK is missing, overproduction of hook protein produces super-polyhooks (144). One idea is that FliK functions with FlhB, a membrane protein of the transport apparatus, to switch the export substrate specificity from hook protein to hook-associated proteins and flagellin once the hook reaches its proper length (142, 145). What the signal might be that triggers this transition or why FliK export is required is not clear. Another idea, suggested by the fact that some mutations in genes encoding C-ring proteins produce short hooks, is that the C-ring has a set capacity for hook protein, which is exported en bloc (146). Somehow, this triggers secretion of FliK, which switches the export substrate specificity to flagellin. Again, how this might happen is not clear.

The hook-associated proteins (147) are added in the order HAP1 (FlgK), HAP3 (FlgL), and HAP2 (FliD). Finally, the FliC subunits (flagellin) required for growth of the filament are inserted under a cap (FliD) at its distal end (148, 149). Mutants that lack the cap simply dump flagellin into the external medium (150).

One can polymerize flagellin onto FlgL in such mutants by adding it exogenously (151, 152) or grow filaments in the normal fashion by supplementing such mutants, either with endogenous FliD (153) or with FliD preassembled into the cap structure (154). The cap promotes polymerization of flagellin; it has five legs that leave room for only one flagellin subunit at a time, and it counter rotates to accommodate insertion of additional subunits, one after another (155). Filament extension appears to be limited by the rate of flagellin export because filaments grow at a rate that decreases exponentially with length (156). For a recent review of the mechanism of filament assembly, see (157).

Presumably the torque-generating units, MotA and MotB, can be incorporated into the structure anytime after class 3 genes are expressed. Motors that are paralyzed because MotA or MotB is missing or defective (with defects induced genetically or mechanically) can be repaired by expression of functional copies; see below. When MotA and MotB are expressed together, they do not make membranes leaky to protons, as judged by the lack of any impairment of growth (158). No mutants have been found that implicate specific binding sites for MotB on other components of the flagellar motor; MotB simply has a peptidoglycan binding motif (59). These considerations have led to an ingenious model in which the periplasmic tails of MotB block proton channels in the MotA/MotB complex until the complex finds itself oriented properly at the periphery of the flagellar motor. Then the periplasmic tails bind to the peptidoglycan, thereby opening the proton channels (159).

FUNCTION

Power Source

Flagellar motors of *E. coli* and *S. typhimurium* are powered not by ATP (160) but rather by protons moving down an electrochemical gradient. Other cations and anions have been ruled out (161–163). The work per unit charge that a proton can do in crossing the cytoplasmic membrane is the protonmotive force, Δp. In general, it comprises two terms, one due to the transmembrane electrical potential difference, $\Delta \psi$, and the other to the transmembrane pH difference $(-2.3 \, kT/e) \, \Delta$pH, where k is Boltzmann's constant, T the absolute temperature, and e the proton charge. At 24°C, $2.3 \, kT/e = 59$ mV. By convention, $\Delta \psi$ is the internal potential less the external potential, and ΔpH is the internal pH less the external pH. *E. coli* maintains its internal pH in the range 7.6 to 7.8. For cells grown at pH 7, $\Delta p \approx -170$ mV, $\Delta \psi \approx -120$ mV, and $-59 \, \Delta$pH ≈ -50 mV. For cells grown at pH 7.6 to 7.8, $\Delta p \approx -140$ mV. For a general discussion of chemiosmotic energy coupling, see Harold & Maloney (164).

The dependence of speed on voltage has been measured in *E. coli* by wiring motors to an external voltage source. Filamentous cells were drawn roughly halfway into micropipettes, and the cytoplasmic membrane of the segment of the

cell inside the pipette was made permeable to ions by exposure to gramicidin S. An inert marker was attached to a flagellar motor on the segment of the cell outside the pipette, and its motion was recorded on videotape. Application of an electrical potential between the external medium and the inside of the pipette (the latter negative) caused the marker to spin (165). The rotation speed was directly proportional to Δp over the full physiological range (up to -150 mV). These experiments were done with large markers (heavy loads) at speeds less than 10 Hz. They are being repeated in a different way with small markers (light loads) at speeds up to nearly 300 Hz. So far, the rotation speed still appears proportional to Δp, or to be more precise, to $\Delta \psi$ (C. Gabel & H.C. Berg, unpublished data).

Motors slow down at extremes of pH (usually external pH), below 6 or above 9. This effect is true both for cells tethered to glass by a single flagellum (166–168) and for swimming cells (161, 162, 167, 169). However, swimming cells show thresholds below which cells do not swim ($\Delta p \approx -30$ mV) and above which speed saturates ($\Delta p \approx -100$ mV), neither of which is evident with tethered cells. These thresholds might be due to problems with bundle formation and changes in filament shape, respectively.

The only measurement of proton flux that has been made is with motors of the motile *Streptococcus* sp. strain V4051 (170), a peritrichously flagellated, primarily fermentative, gram-positive organism that lacks an endogenous energy reserve and is sensitive to ionophores and uncouplers. Unlike *E. coli*, this organism can be starved and artificially energized, either with a potassium diffusion potential (by treating cells with valinomycin and shifting them to a medium with a lower concentration of potassium ion) or with a pH gradient (by shifting cells to a medium of lower pH); see Manson et al. (171, 172). If cells are energized in this way in a medium of low buffering capacity, one can follow proton uptake by the increase in external pH. The frequency of rotation of filaments in flagellar bundles can be determined by monitoring the swimming speed—the experiments were done with a smooth-swimming mutant—given the ratio of swimming speed to bundle frequency determined separately by video-taping cells under phase-contrast microscopy and measuring their vibration frequencies by power spectral analysis; see Lowe et al. (173). Finally, the data can be normalized to single motors by counting the number of cells and the number of flagellar filaments per cell. The total proton flux into the cell is much larger than the flux through its flagellar motors. However, the two can be distinguished by suddenly stopping the motors by adding an antifilament antibody—this cross-links adjacent filaments in the flagellar bundles (174)—and measuring the change in flux. This change was found to be directly proportional to the initial swimming speed, as would be expected if a fixed number of protons carries a motor through each revolution. This number is about 1200 (175). One might do better by patch-clamping motors, provided that one could devise a means for monitoring speed. For example, it should be possible to patch-clamp flagella from protoplasts obtained from gram-positive cells by treatment with a suitable muramidase [see, for example, Weibull (176)], but how would one

follow the rotation of elements of the stator, now free of attachment to the rigid framework of the cell wall? Another problem is the small proton flux. The top speed encountered in the experiments just described (175) was 65 Hz, corresponding to a flux of 7.8×10^4 protons per motor per second, or a current of 1.2×10^{-2} pA. Currents flowing through single channels from excitable animal cell nerve membranes are typically 100 times larger.

Some bacteria, notably marine bacteria or bacteria that live at high pH, use sodium ions instead of protons (177, 178). Thus, flagellar motors can be ion driven, not only proton driven. Some Mot components of the motor of the marine bacterium *Vibrio alginolyticus* are homologous to MotA and MotB, namely PomA and PomB, but others are not, namely MotX and MotY (179). When flagella are driven with a large sodium gradient, their rotation speeds can be remarkably high, up to 1700 Hz (180, 181). And rotation can be blocked with specific inhibitors of sodium transport, such as amiloride (182) or phenamil (183). This property has made it possible to screen for sodium-channel mutants (184, 185). Also, functional chimeras have been constructed using components from proton- and sodium-ion-driven motors (see, for example, References 186, 187).

Torque-Generating Units

The flux through the flagellar motor is divided into as many as eight distinct proton channels (or pairs of proton channels), comprising one or more copies of the proteins MotA and MotB (currently thought to be 4 MotA and 2 MotB). It was shown by Stocker et al. (188) in the early days of bacterial genetics that phage grown on motile strains of *Salmonella* could transduce flagellar characters into nonmotile strains. Silverman et al. (189) utilized λ transducing phage to "resurrect" nonmotile mutants of *E. coli,* a process that occurred more rapidly when the basal body was already assembled and only *mot* genes needed to be transferred. Such activation was studied at the level of a single motor by Block & Berg (190), who tethered *motB* cells to a glass surface by a single flagellum (191) and expressed the wild-type gene from a plasmid under control of the *lac* promoter—λ phage was tried but did not work, because the phage heads adhered to the glass surface and prevented tethered cells from rotating (S.M. Block & H.C. Berg, unpublished data). This work was extended to *motA* cells in a more carefully controlled study by Blair & Berg (192). The speed of a tethered cell increased in a number of equally spaced steps, as shown in Figure 4, indicating that each additional torque-generating unit (comprising MotA and MotB) adds the same increment of torque (applies a similar force at the same distance from the axis of rotation). The main argument for a complement of 8 such torque-generating units is that resurrections of this kind have produced 8 equally spaced levels more than once, but never 9. As noted above in the section on structure, the number of studs seen in freeze-fracture experiments range from about 10 to 16. In particular, the number seen for *E. coli* is 10–12 (51). Blair & Berg (192), wondering whether this might represent an incomplete set, produced MotA and
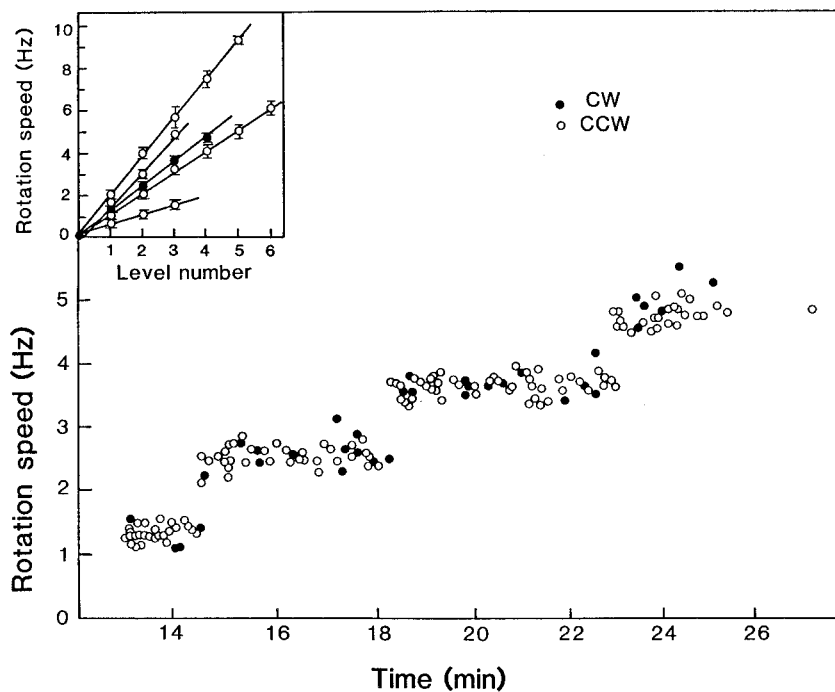
Figure 4   Rotation speed of a tethered *motA* cell, *E. coli* strain MS5037(pDFB36),
following addition (at time 0) of the inducer IPTG (added in a minimal medium
containing glycerol, glucose, and essential amino acids). Filled circles indicate CW
rotation, open circles CCW rotation. The inset shows the mean rotation speed (plus
or minus the standard error of the mean) at each level (step of the staircase) as a
function of level number for this cell (closed circles) and for four additional cells
(open circles). (From Reference 192, Figure 1, reprinted with permission from the
American Association for Advancement of Science.)

MotB at a slight excess of wild-type levels and found that the torque increased by
about 20%. They also found that the torque for wild-type motors was only about 5
times that for a one-generator motor, whereas following complete resurrection, this
factor was about 8. So it is possible that the full complement of torque generators is
8, and the full complement of studs is 16, which yields 2 studs per torque generator.

Stepping

It is likely that the passage of each proton (or each proton pair) moves a torque
generator (a MotA/MotB complex) one step (one binding site) along the periph-
ery of the rotor, suddenly stretching the components that link that generator to the
rigid framework of the cell wall. As this linkage relaxes, a tethered cell should

rotate by a fixed increment. In other words, this molecular machine should behave like a stepping motor. Since proton passage is likely to occur at random times, the steps will occur with exponentially distributed waiting times. We have been looking for such steps since 1976 (193) but without success. The main reason, advanced then, is that the torque applied to the structure linking the rotor to the tethering surface (a series of elastic elements, comprising the rod, hook, and filament) causes that structure to twist (for measurements of the torsional compliance, see References 194, 195). When less torque is applied, these elements tend to untwist, carrying the cell body forward. Therefore, discontinuities in the relative motion of rotor and stator are smoothed out. To succeed, one probably needs to work at reduced torque, e.g., with a one-generator motor driving a small viscous load, perhaps just a hook. Such an object is expected to spin quite rapidly, so the technical problems are formidable.

One route around this difficulty is to examine variations in rotation period. If n steps occur at random over each revolution, then the ratio of the standard deviation to the mean should be $n^{-1/2}$ (196, p. 24; 197, appendix). An early analysis of this kind led to an estimate of $n \approx 400$ (198), which has been borne out by more recent work (197). The more recent analysis also showed that a tethered cell is restrained: It is not free to execute rotational Brownian motion. Thus, the rotor and stator are interconnected most of the time.

This stochastic analysis was repeated with tethered cells undergoing resurrection (as in Figure 4), and the number of steps per revolution was found to increase linearly with level number, increasing by about 50 steps per level (199). If torque generators interact with a fixed number of binding sites on the rotor, say 50, then why is the number of steps per revolution not just 50? If m torque generators are attached to the rotor and one steps, suddenly stretching its linkage to the rigid framework of the cell wall, then when that linkage relaxes and moves the rotor, it also must stretch the linkages of the $m - 1$ torque generators that have not stepped. If $m = 2$, the net movement of the rotor is half of what it would be at $m = 1$, so the apparent step number is 100 per revolution. If $m = 8$, the apparent step number is 400 per revolution. If, on the other hand, each torque generator is detached most of the time (for most of its duty cycle), then the apparent step number would remain 50. So, this experiment argues not only that each force generator steps independently of all the others, but that each remains connected to the rotor most of the time. In fact, the torque generators must be attached nearly all of the time; see below.

If steps occur at random, then the numbers 50, 100, . . . , 400 all are lower bounds. The smoother the rotation, the larger the estimate of the number of steps per revolution. Therefore, any noise in the system that adds to variation in rotation period reduces that estimate. If steps do not occur at random, i.e., if steps are clocked or successive steps are not independent of one another, then similar statistics could be generated with fewer steps; see Svoboda et al. (200).

Coarser fluctuations, probably associated with variations in the number of active torque-generating units, have been studied by Kara-Ivanov et al. (201).
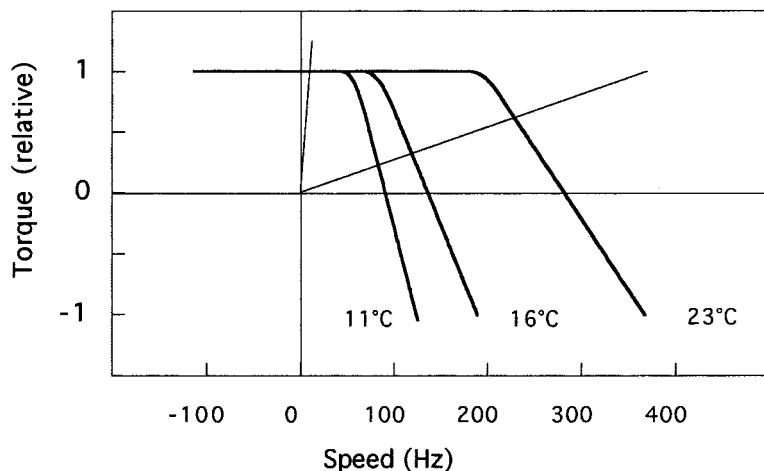
Figure 5   The torque-speed curve for the flagellar motor of *E. coli* shown at three temperatures (thick lines), together with two load lines (thin lines), one for an object the size of the cell body of wild-type *E. coli* (effective radius about 1 μm, left), the other for a minicell (effective radius about 0.3 μm, right). The strains used were derived from *E. coli* wild-type strain AW405 (219). Later work (203) showed that the torque declines somewhat in the low-speed regime, by about 10% between stall and the knee; see the text. (Adapted from Reference 202, Figure 16.)

Torque-Speed Dependence

A crucial test of any rotational motor model is its torque-speed dependence. Measurements of the torque generated by the flagellar motors of *E. coli* have been made over a wide range of speeds, including speeds in which the motor is driven backward, with the results shown in Figure 5. At 23°C, the torque exerted by the motor is approximately constant, all the way from negative speeds of at least -100 Hz to positive speeds of nearly 200 Hz. At higher speeds it declines approximately linearly, crossing the 0-torque line at about 300 Hz. At lower temperatures, the region of transition from constant torque to declining torque—we call this the "knee"—shifts to lower speeds, and the region of decline steepens (202, 203); the latter parts of the curves can be mapped onto one another with scaling of the speed axis.

Estimates of the torque generated in the low-speed regime range from about 2.7×10^{-11} dyn cm (2700 pN nm) to 4.6×10^{-11} dyn cm (4600 pN nm), the smaller value from estimates of the viscous drag on tethered cells of *Streptococcus* (173) and the larger value from the force exerted by tethered cells of *E. coli* on latex beads held in an optical trap (204).

A motor driving an inert object (a cell body, a latex bead, etc.) will spin at the speed at which the torque generated by the motor is balanced by the torque exerted on the object by viscous drag. The latter torque is defined by load lines,

such as those shown in Figure 5 (thin lines), the one at the left for a large object and the one at the right for a small object. To appreciate this concept, note that the torque, N, required to rotate an object of fixed shape in a viscous medium is its rotational frictional drag coefficient, f, times its angular velocity, Ω (2π times its rotation speed, in Hz). In a torque versus speed plot, this function is a straight line passing through the origin, with slope f. Here, we assume that the medium is Newtonian, i.e., that the frictional drag coefficient does not depend on Ω, a condition satisfied in a dilute aqueous medium that does not contain long unbranched molecules, such as methylcellulose or polyvinylpyrrolidone (205). For such a medium, f is a geometrical factor times the bulk viscosity, η, where η is independent of Ω (independent of the rate of shear). For an isolated sphere of radius a spinning about an axis through its center, for example, this geometrical factor is $8\pi a^3$. For compact globular objects, the actual shape is not very critical; however, accurate values can be computed (206). The distance from the tethering surface does not really matter, either, provided that the gap between the object and the surface is at least 0.2 cell radii (193, 207).

At 23°C and for the load line shown at the left in Figure 5, the motor runs at 10 Hz; for the load line shown at the right, it runs at about 220 Hz. For a very shallow load line, e.g., one for a free hook, the speed would be close to the zero-torque speed, about 290 Hz. A motor free-running in this way always operates in the upper right quadrant of Figure 5. It cannot drive itself backward; however, it can redefine what is meant by forward by switching from CCW to CW or back again. Nor can it spin faster than its speed at zero load. To probe the upper left or lower right quadrants of Figure 5, one needs to subject the motor to torque applied externally.

One way to do this is by electrorotation (208). Cells were tethered and exposed to a high-frequency (2.25 MHz) rotating electric field (202). As explained in the cited reference, the external electric field polarizes the cell. The dipole field due to the polarization rotates at the same rate and in the same direction as the applied electric field. However, because of the finite time required for redistribution of charges, the polarization vector leads or lags the electric-field vector. The externally applied torque is the cross product of these vectors. The applied torque varies as the square of the magnitude of the electric field and changes sign with changes in the direction of rotation of that field. Therefore, it is possible to spin a tethered cell either forward or backward. Speeds of several hundred Hz are readily attainable (202). For reasons that we do not understand, the motor of a cell driven backward (CW if it is trying to spin CCW, or CCW if it is trying to spin CW) often breaks catastrophically: Motor torque suddenly drops to zero, the cell appears free to execute rotational Brownian motion, and the motor fails to recover. Our best guess is that the C-ring is sheared off the bottom of the rotor (Figure 1), disengaging all torque-generating units but leaving the bearings intact. If one were to break the rod, the cell would simply come off the tethering surface. We know this because certain mutations in the gene for the MS-ring weaken the rod MS-ring attachment, allowing rod, hook,

and filament to pull out of the cell (209). In any event, once the motor has broken, one can compare the speed at which the cell body turns at a given value of externally applied torque with the speed at which it turned at the same value of externally applied torque before the break occurred. That difference is proportional to the torque generated by the motor at the speed at which it turned when intact. The data shown by the thick lines in Figure 5 were determined in this way. Difficulties encountered along the way are described elsewhere (210, 211). In particular, we had thought that there might be a barrier to backward rotation, but this proved to be an artifact due to ellipticity in the applied electric field. The possibility of a barrier was ruled out in experiments utilizing optical tweezers (204).

Additional work on the behavior of the motor in the upper right quadrant of Figure 5 was done by manipulating load lines. Flagella were shortened by viscous shear, and cells were adsorbed onto positively charged glass. Latex beads of various sizes were attached to the flagellar stubs, and the slopes of their load lines were increased by addition of the Ficoll (203). In the low-speed regime, torque was found to drop by about 10% from zero speed (stall) to the knee. In this regime, torque was independent of temperature, and solvent isotope effects (effects if shifts from H_2O to D_2O) were relatively small, as found earlier for artificially energized cells of *Streptococcus* (212). Evidently, at low speeds the motor operates near thermodynamic equilibrium, where rates of displacement of internal mechanical components or translocation of protons are not limiting. In the high-speed regime, torque was strongly temperature dependent, as seen in Figure 5, and solvent isotope effects were large (168), as found earlier for swimming cells of *E. coli, S. typhimurium,* and *Streptococcus* (173, 175, 213). This is what one would expect if the decline in torque at high-speed results from limits in rates of proton transfer (proton dissociation).

Slowly declining torque in the low-speed regime argues for a model in which the rate-limiting step depends strongly on torque and dissipates most of the available free energy, that is, for a powerstroke mechanism. The absence of a barrier to backward rotation rules out models (e.g., thermal ratchets) that contain a step that is effectively irreversible and insensitive to external torque (210). Eventually, we would like to understand why the low-speed regime is so broad, why the boundary between the low-speed and high-speed regimes is so narrow, and why the position of that boundary is sensitive to temperature.

The power output, the power dissipated when a torque N sustains rotation at angular velocity Ω, is $N\Omega$. For a torque of 4600 pN nm and a speed of 10 Hz, this is 2.9×10^5 pN nm s^{-1}. The power input, the rate at which protons can do work, is proton flux times proton charge times protonmotive force. Assuming 1200 protons per revolution and speed 10 Hz, the proton flux is 1.2×10^4 s^{-1}. For *E. coli* at pH 7, $\Delta p \approx -170$ mV. Therefore, the power input is $(1.2 \times 10^4$ s$^{-1}) (e) (0.17$ V$) = 2.0 \times 10^3$ eV s^{-1}, where e is the proton charge. Since 1 eV (one electron volt) $= 1.6 \times 10^{-12}$ erg $= 160$ pN nm, the power input is 3.2×10^5 pN nm s^{-1}. Therefore, by this crude estimate, the efficiency of the

motor, power output divided by power input, is about 90%. Within the uncertainty of the measurements—the proton flux has not been measured in *E. coli*—the efficiency could be 1, the value expected for a tightly coupled engine running slowly close to stall (175).

The power output, $N\Omega$, increases linearly with speed up to the boundary between the low-speed and high-speed regimes, and then it declines. If a fixed number of protons carries the motor through each revolution, the power input also increases linearly with speed. Therefore, the efficiency remains approximately constant up to the knee, and then it declines. There is no discontinuity in torque as one crosses the zero-speed axis (204). As the motor turns backward, it must pump protons, just as the F_0-ATPase pumps protons when driven backward by F_1.

The force exerted by each force-generating unit is substantial but not large on an absolute scale. If we take a ballpark figure for the stall torque of 4000 pN nm and assume that force-generating units act at the periphery of the rotor at a radius of about 20 nm, then 200 pN is applied. If there are 8 independent force-generating units, then each contributes 25 pN. This force is about equal in magnitude to that between two electrons 4.8 Å apart in a medium of dielectric constant 40 (midway between water, 80, and lipid, about 2). So, almost any kind of chemistry will do.

The energy available from one proton moving down the electrochemical gradient is $e\Delta p$. Given $\Delta p \approx -170$ mV, this is 0.17 eV, or 27 pN nm. At unit efficiency, this equals the work that the force-generator can do, Fd, where F is the force that it exerts, and d is the displacement generated by the transit of one proton. Assuming 52 steps per revolution (twice the number of FliG subunits) and a rotor radius of 20 nm, $d \approx 2.4$ nm. So $F \approx 11$ pN. If two protons are required per elementary step, the force is twice as large, and $F \approx 22$ pN. So the displacement of 2 protons per step is likely.

Angular Dependence of Torque

When optical tweezers were used to drive cells slowly backward or to allow them to turn slowly forward (204), torque did not vary appreciably with angle. When the motor is fully energized and has a full complement of torque-generating units, there is no discernible periodic fluctuation. On the other hand, the rotation rates of tethered cells often peak at some point in the cycle and pass through a minimum one-half revolution away. But this behavior is to be expected for cells tethered near one end when the axis of the tether is not normal to the plane of the glass. A very different result is obtained when one energizes and de-energizes tethered cells and asks where they stop or watches them spin when the proton-motive force is very low. When this manipulation was done with *Streptococcus,* periodicities were observed of order 5 or 6 (214). This probably reflects small periodic barriers to rotation intrinsic to the bearings.

Duty Ratio

In our stochastic analysis of steps (in the earlier section Stepping), we argued that the apparent number of steps per revolution would increase with the number of torque generators, as observed, if each torque generator remained attached to the rotor most of the time, i.e., if the torque-generating units had a high duty ratio. This issue was addressed directly in an experiment in which motors were resurrected at low viscous loads (215). If each unit remains attached to the rotor for most of its mechanochemical cycle, then near zero load, one generator can spin the rotor as fast as two or more. The speed is limited by the rate at which the first torque-generating unit can complete its mechanochemical cycle. The smallest load studied was that of a 0.3-μm-diameter latex sphere, and the best we could do was to conclude that the duty ratio was greater than 0.6.

In fact, the duty ratio must be close to 1; i.e., torque generators, like molecules of kinesin, are processive. The argument goes as follows: Consider a tethered cell driven by a single torque-generating unit, as in the first step of the resurrection shown in Figure 4. If a wild-type motor with 8 torque-generating units generates a torque of about 4×10^{-11} dyn cm (4000 pN nm), then the single-unit motor generates a torque of about 5×10^{-12} dyn cm. The torsional spring constant of the tether (the compliance is mostly in the hook) is about 5×10^{-12} dyn cm rad^{-1} (194), so the tether is twisted up about 1 radian, or 57°. Now, the viscous drag on the cell body is enormous compared to that on the rotor, so if the torque-generating unit lets go, the tether will unwind, driving the rotor backward. If the single unit steps 50 times per revolution, the displacement is 7.2° per step. If the cell is spinning ~1.2 Hz (Figure 4), the step interval is 1.6×10^{-2} s. If the duty ratio is 0.999, so that the torque-generating unit detaches for 1.6×10^{-5} s during each cycle, how far will the tether unwind? The tether unwinds exponentially: $\theta = \theta_0 \exp(-\alpha t)$, where θ_0 is the initial twist and α is the torsional spring constant divided by the rotational frictional drag coefficient. If we approximate the rotor as a sphere of radius $a = 20$ nm immersed in a medium of viscosity $\eta = 1$ P (1 g cm^{-1} s^{-1}), which is about right for a lipid membrane, then the frictional drag coefficient, $8\pi\eta a^3$, is 2×10^{-16} dyn cm per rad s^{-1}, and $\alpha = 2.5 \times 10^4$ s^{-1}. So, in 1.6×10^{-5} s, the twist in the tether decreases from 57° to 57° $\exp(-2.5 \times 10^4$ s$^{-1} \times 1.6 \times 10^{-5}s) = 38°$, or by 19°, i.e., by more than twice the step angle. Thus, the torque-generating unit would not be able to keep up. So the duty ratio must be close to 1. The interaction between the torque-generating unit and the rotor must be such that the rotor is not able to slip backward. If one imagines that a torque-generating unit binds to successive sites along the periphery of the rotor, then it has no unbound states. If each torque-generating unit has two proton channels, it is possible that a MotA associated with one channel remains attached to a FliG, while the MotA associated with the other channel takes the next step.

Switching

If one follows the direction of rotation of tethered cells and plots CW and CWW interval distributions, the plots are, to a first approximation, exponential. This

relationship is true even during responses to constant chemotactic stimuli (216). Exceptions might apply to short events that are difficult to observe (217), and to long events that fall outside the time span of the usual measurements. Also, cells occasionally pause, particularly when the CW bias is high, for example, when responding to repellents (218). In our experiments done with wild-type *E. coli* strain AW405 (219) to a resolution of about 50 ms (220), pauses occur at a frequency of at most 3% of all events, including changes in direction, pauses, and events in which cells might, instead, stick to the tethering surface (S.M. Block & H.C. Berg, unpublished data). So, right or wrong, we have not considered pauses to be very important for chemotactic behavior. To deal properly with short events and pauses, one probably needs better time and spatial resolution than available with standard video. And then one needs to think hard about artifacts introduced by twisting of the tether, Brownian motion, and missed events.

When switching occurs, it appears to be all-or-none: One does not see motors step through an intermediate set of angular velocities, as would be expected if different force-generating units were to switch independently. With tethered cells, the time delay is no more than 10 ms, including the time required for the tether to untwist and then twist up again in the opposite direction (193). With single filaments observed by laser light scattering, reversals appear to be complete within 1 ms (221). If different torque-generating units are to switch synchronously, a global conformational change must occur that involves the arrays of sites with which MotA and MotB interact, probably through flexing of the MS- and/or C-rings (222). This conclusion is consistent with the biochemical and genetic evidence, discussed earlier, in which CheY-P binds to FliM and in which FliG, FliM, and FliN constitute a switch complex.

It was suggested by Khan & Macnab (161) and reaffirmed by Macnab (44) that switching is a thermal isomerization, in which the system sits in one of two potential wells and, with exponentially distributed waiting times, jumps from one to the other. Let the free energies of the CCW and CW states be G_{CCW} and G_{CW} and the free energy of the intervening transition state be G_T. The transition rate constants between the CCW and CW states, k^+ and k^-, are characterized by a factor that represents the frequency at which the system tries to jump, and a factor that represents the probability that it has enough energy to cross the activation barrier $G_T - G_{CCW}$ or $G_T - G_{CW}$. The ratio of the probabilities of the CW or CCW state, (CW bias)/(1 − CW bias) = $k^+/k^- = \exp(-\Delta G/kT)$, where $\Delta G = G_{CW} - G_{CCW}$ (defined in units of kT, the energy of thermal fluctuation for one particle, i.e., Boltzmann's constant times absolute temperature).

Strains that do not express the signaling molecule, CheY, or the kinase required for its phosphorylation, CheA, rotate exclusively CCW, so in the absence of CheY-P, G_{CCW} is much smaller than G_{CW}. However, the relative depths of these wells can be shifted by lowering the temperature (223). CW intervals appear at about 10°C and become as long as CCW intervals at about −1°C. ΔG changes linearly with temperature. An extrapolation back to room

temperature (23°C) yields a value there of 14.4 kT. A similar effect on the free energies of the CW and CCW states has been found on varying the intracellular concentration of fumarate (224).

Several recent studies have addressed the question of how this state of affairs is perturbed by chemotactic signaling. In one study, CheY was replaced by the double-mutant CheY(D13K Y106W), abbreviated CheY**, a protein active without phosphorylation, in a strain lacking the kinase CheA and the phosphatase CheZ (225). In a second study, CheY was expressed in a strain in which all of CheY is phosphorylated, a strain that has the kinase but lacks the phosphatase and the receptor-demethylating enzyme CheB (226). In both cases, plots of CW bias versus CheY concentration were sigmoidal and could be characterized by Hill coefficients of 4.2 and 2.5, respectively. However, this nonlinearity arises not from the binding per se but from the effect of the binding of CheY** or CheY-P to FliM. Scharf et al. (225) assumed linear binding and found that ΔG decreased by about $r = 0.8 \, kT$ for each molecule of CheY** bound, with the level of the CCW state rising and the level of the CW state falling by similar amounts, 0.4 kT. Alon et al. (226) used the allosteric model of Monod et al. (227), which could be fit with dissociation constants for binding in the CW (or tight) state, K_T, and in the CCW (or relaxed) state, K_R, that differed by a factor of about 2. The two results are equivalent, since $r = kT \ln(K_R/K_T)$. That is, both treatments assume that probabilities of switching are affected by stabilization of the CW state relative to the CCW state. Scharf et al. treat the flagellar motor as an open system and proceed phenomenologically, with r a free parameter. They do not specify a mechanism for the energy shift. Alon et al. treat the flagellar motor as a closed system, with r determined by the difference in binding affinities between tight and relaxed states. The models make similar predictions, because the latter differences are small. In more recent work, the energy shift, r, has been determined over a range of temperatures. It increases linearly from about 0.3 kT at 5°C to about 0.9 kT at 25°C (228).

A third study, done with individual cells rather than with cell populations, revealed a much steeper motor response, characterized by a Hill coefficient of 10.3 (229). CheY-GFP (green fluorescent protein) was expressed in the strain used by Alon et al., in which all CheY is phosphorylated. The CheY-GFP concentration was measured in single cells by fluorescence correlation spectroscopy, and the rotational behavior of a bead attached to a single flagellar filament was monitored. All of the data obtained from different cells expressing different levels of CheY-GFP fell on the same curve, shown in Figure 6 (open triangles, right ordinate). The dashed line is a fit to the allosteric model (227). Also shown in this figure is a binding curve of CheY-P to FliM, obtained from measurements of fluorescence resonance energy transfer (FRET) between CFP-FliM and CheY-YFP (230). The binding is approximately linear (closed circles, left ordinate, $K_D = 3.7 \pm 0.4 \, \mu M$, Hill coefficient 1.7 ± 0.3) but also can be fit to the allosteric model (dashed line). The dissociation constants for the two fits are given in the
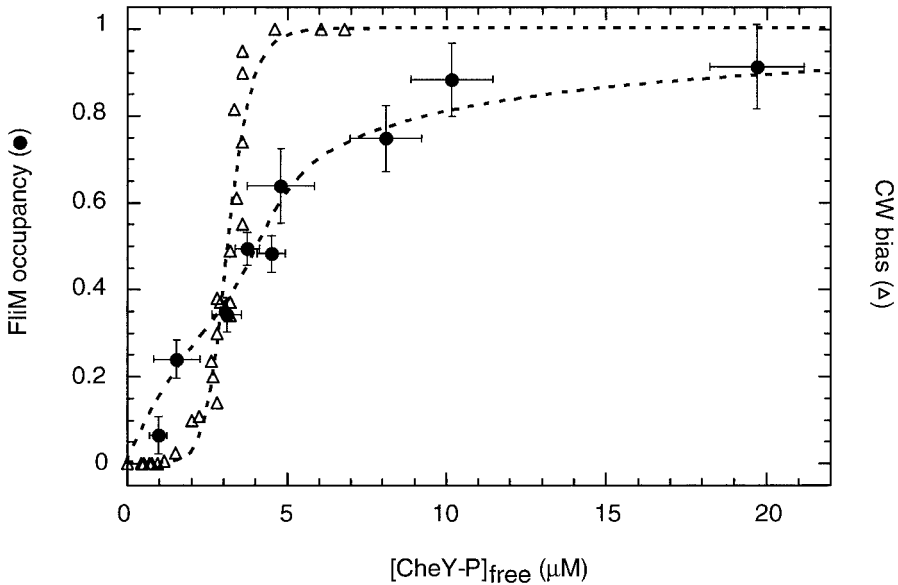
Figure 6   Comparison of dependence of motor bias (△) and FliM occupancy (●) on concentration of free cytoplasmic CheY-P. Dashed lines are fits to the allosteric model: for motor response, $K_T = 2.3 \pm 0.6\ \mu M$, $K_R = 6.6 \pm 3.0\ \mu M$; for binding, $K_T = 2.4 \pm 0.2\ \mu M$, $K_R = 5.7 \pm 1.0\ \mu M$. (Data for the motor bias are from Reference 229 and for the FliM binding from Reference 230. Adapted from Reference 230, Figure 2b.)

figure legend. As before, values for the CW and CCW states differ by a factor of about 2. (For other means of observing the binding of CheY-P to the base of the flagellar motor, see Reference 231.)

A more general stochastic model has been developed in which a ring of proteins (34 copies of FliM) display cooperative interactions (232). Each protein, or protomer, can adopt a CW or CCW configuration, and the direction of rotation depends upon how many protomers are in either state. Given a large enough coupling energy between adjacent protomers, the ensemble switches from a state in which nearly all of the protomers are in the CW configuration to one in which nearly all of the protomers are in the CCW configuration. As before, the motor response is more nonlinear than the binding. This model readily accommodates pauses, which are frequent when the coupling energy is small and the protomers tend to behave independently.

None of this tells us how the shapes of the C- or MS-rings differ in the CCW or CW states or how the binding of CheY-P to FliM stabilizes one conformation and destabilizes the other. We need to learn more about the structures of FliG, FliM, and FliN and the dynamics of their interactions.

MODELS

The fundamental question is how the flagellar motor generates torque, namely, how inward motion of one or more ions through a torque-generating unit causes it to advance circumferentially along the periphery of the rotor. Once that is understood, the nature of the conformational change required for switching, namely, how the direction of advance is distinguished from that of retreat, is likely to be self-evident. Criteria for success in modeling should be based on the behavior of individual motors, not groups of motors, as reflected in the way peritrichously flagellated bacteria swim. As is apparent in Figure 3, cell behavior is complicated by polymorphic transformations of the flagellar filaments.

Moving parts of the motor are submicroscopic and immersed in a viscous medium (water or lipid), so the Reynolds number is very small (233–236). And everything is overdamped (see Reference 237, pp. 41–45). So the designer does not have the benefit of flywheels or tuning forks. If, for example, the operator of the motor driving a tethered cell of *E. coli* 10 Hz were to disengage in the clutch, the cell body would coast no more than a millionth of a revolution (24). So, if there is a stage in the rotational cycle in which the torque changes sign, the motor will stop. Predicting net torque after averaging over a complete cycle is not sufficient. And mechanisms in which energy is stored in vibrational modes are not viable. However, one can use energy available from an electrochemical potential to stretch a spring and then use that spring to apply a steady force. As we have seen, the force required is modest, and almost any kind of chemistry will do.

Motion of the torque-generating units relative to the periphery of the rotor is driven by a proton (or sodium-ion) flux. Only one experiment has attempted to measure this flux (175), and flux and speed were found to be linearly related. Unless protons flow through the motor when it is stalled, this implies that a fixed number of protons carry the motor through each revolution. The running torque at low speeds is close to the stall torque (Figure 5). If the motor is stalled and no protons flow, no free energy is dissipated; therefore, the stalled motor is at thermodynamic equilibrium. For slow rotation near stall, the motor must operate reversibly at unit efficiency, with the free energy lost by protons traversing the motor equal to the mechanical work that it performs. This implies that the torque near stall should be proportional to the protonmotive force over its full physiological range, as observed. So the evidence is consistent with a model in which the motor is tightly coupled.

An important question is whether the ion that moves down the electrochemical gradient is directly involved in generating torque, i.e., participates in a power-stroke in which dissipation of energy available from the electrochemical gradient and rotational work occur synchronously, or whether the ion is indirectly involved in generating torque, e.g., by enabling a ratchet that is powered thermally. In the powerstroke case, protons can be driven out of the cell by backward rotation and steep barriers are not expected. In addition, if the

rate-limiting step is strongly torque dependent, then the torque-speed curve (as plotted in Figure 5) can have a relatively flat plateau, because small changes in torque can generate large changes in speed (238) (see Reference 210, Figure 6c). In the ratchet case, with tight coupling, the likelihood of transit of ions against the electrochemical gradient is small, so the system must wait, even when large backward torques are applied, and barriers to backward rotation are expected. Also, the torque-speed curves are relatively steep (167) (see Reference 210, Figure 6b). So, the torque-speed curves of Figure 5 favor a powerstroke mechanism.

Tightly coupled models can be distinguished from one another only by their behavior at high speeds, far from the point of thermodynamic equilibrium. A seminal test for any such model is the torque-speed curve of Figure 5. The thermal-ratchet model that we proposed (222, 239), which (with improvements) has been applied successfully to F_0 (240), fails this test. At negative speeds, it predicts barriers to rotation, and at positive speeds, it predicts a torque that falls steadily toward the zero-torque speed. It does not predict a constant-torque plateau or an abrupt transition from a low-speed to a high-speed regime (see Reference 222, Figure 7).

As argued in the section on duty ratio, a torque generator must not have unbound states, i.e., states in which the rotor is free to spin backward. The ratchet model meets this criterion, even though its channel complex is not bound to the rotor in the usual biochemical sense. It is simply free to move forward or backward one step at a time, depending upon the occupancy of adjacent proton-accepting sites.

Finally, a successful model must be consistent with the general structural features outlined in Figure 1, where the filament, hook, rod, MS-ring, and FliG rotate relative to the rigid framework of the cell, defined by the peptidoglycan layer, and the Mot proteins do not. FliM and FliN are likely part of the rotor; however, the evidence for this is not airtight. Since MotA and B are embedded in the cytoplasmic membrane, they are not free to execute movements out of the plane of that membrane. Their movements are presumably cyclic. One can imagine a model in which a MotA/MotB complex rolls along the periphery of the rotor, but not if more than one MotB is bound to the peptidoglycan.

There appear to be essential electrostatic interactions between specific residues in the cytoplasmic domain of MotA and the C-terminal domain of FliC (69). Here, charge complementarity is more important than surface complementarity, i.e., long-range interactions appear to be more important than tight binding. Since some models for torque generation require transfer of protons from the stator to the rotor, it was expected that acidic residues on FliG might be more important than basic residues. However, replacement of the acidic residues deemed important for torque generation with alanine still allowed some rotation, whereas reversing their charge had a more severe effect (68). An extension of this study failed to identify any conserved basic residues critical for rotation in MotA, MotB, FliG, FliM, or FliN and only one conserved acidic residue critical for rotation, Asp32 of MotB (70). Other alternatives were considered and either

ruled out or deemed unlikely. Therefore, the only strong candidate for a residue that functions directly in proton conduction is Asp32 of MotB.

Given this work, I would bet on a cross-bridge mechanism of the kind that Blair and colleagues propose (71). In such a scheme, proton transport drives the following cyclic sequence: First, a proton binds to an outward-facing binding site. Second, the protonmotive force drives a conformational change, a power-stroke that moves the rotor forward (or stretches a spring that moves it forward) and transforms the binding site to an inward-facing site. Finally, proton dissociation triggers detachment of the cross-bridge from the rotor, its relaxation to the original shape, and reattachment to an adjacent site. If the MotA/MotB complex is two headed, one head could remain attached while the other stepped, thus ensuring a high duty ratio. The cross-bridge mechanism was analyzed earlier by Läuger (Model II of Reference 241), but at a time when the torque-speed curve was not known to have a plateau, so this work should be revisited. To formulate models adequate for physiological testing, it would help to have more structural information.

REVIEWS

Models proposed for the flagellar motor are cataloged elsewhere (202, 242). Other reviews on the structure and function of proton-driven motors are available (211, 243–251). Also available are reviews on sodium motors (252, 253) and on flagellar genetics and assembly (101, 246, 254–256), as well as tutorials on the mathematical treatment of motor models (249, 257).

ACKNOWLEDGMENTS

The *Annual Review of Biochemistry* is online at http://biochem.annualreviews.org

LITERATURE CITED

1. Larsen SH, Reader RW, Kort EN, Tso W, Adler J. 1974. *Nature* 249:74–77

2. Macnab RM, Ornston MK. 1977. *J. Mol. Biol.* 112:1–30

3. Turner L, Ryu WS, Berg HC. 2000. *J. Bacteriol.* 182:2793–801

4. Blair DF. 1995. *Annu. Rev. Microbiol.* 49:489–522

5. Stock JB, Surette MG. 1996. See Ref. 261, pp. 1103–29

6. Falke JJ, Bass RB, Butler SL, Chervitz SA, Danielson MA. 1997. *Annu. Rev. Cell Dev. Biol.* 13:457–512

7. Stock AM, Robinson VL, Goudreau PN. 2000. *Annu. Rev. Biochem.* 69:183–215

8. Bren A, Eisenbach M. 2000. *J. Bacteriol.* 182:6865–73

9. Falke JJ, Hazelbauer GL. 2001. *Trends Biochem. Sci.* 26:257–65

10. Bray D. 2002. *Proc. Natl. Acad. Sci. USA* 99:7–9

11. Bourret RB, Stock AM. 2002. *J. Biol. Chem.* 277:9625–28

12. Iino T, Komeda Y, Kutsukake K, Macnab RM, Matsumura P, et al. 1988. *Microbiol. Rev.* 52:533–35

13. Asakura S. 1970. *Adv. Biophys.* 1:99–155

14. Calladine CR. 1978. *J. Mol. Biol.* 118:457–79

15. Kamiya R, Asakura S, Wakabayashi K, Namba K. 1979. *J. Mol. Biol.* 131:725–42

16. Fahrner KA, Block SM, Krishnaswamy S, Parkinson JS, Berg HC. 1994. *J. Mol. Biol.* 238:173–86

17. Hasegawa K, Yamashita I, Namba K. 1998. *Biophys. J.* 74:569–75

18. Yamashita I, Hasegawa K, Suzuki H, Vonderviszt F, Mimori-Kiyosue Y, Namba K. 1998. *Nat. Struct. Biol.* 5:125–32

19. Namba K, Vonderviszt F. 1997. *Q. Rev. Biophys.* 30:1–65

20. Samatey FA, Imada K, Nagashima S, Vonderviszt F, Kumasaka T, et al. 2001. *Nature* 410:331–37

21. DePamphilis ML, Adler J. 1971. *J. Bacteriol.* 105:376–83

22. DePamphilis ML, Adler J. 1971. *J. Bacteriol.* 105:384–95

23. DePamphilis ML, Adler J. 1971. *J. Bacteriol.* 105:396–407

24. Berg HC. 1974. *Nature* 249:77–79

25. Ueno T, Oosawa K, Aizawa S-I. 1992. *J. Mol. Biol.* 227:672–77

26. Ueno T, Oosawa K, Aizawa S-I. 1994. *J. Mol. Biol.* 236:546–55

27. Driks A, DeRosier DJ. 1990. *J. Mol. Biol.* 211:669–72

28. Khan IH, Reese TS, Khan S. 1992. *Proc. Natl. Acad. Sci. USA* 89:5956–60

29. Francis NR, Sosinsky GE, Thomas D, DeRosier DJ. 1994. *J. Mol. Biol.* 235:1261–70

30. Katayama E, Shiraishi T, Oosawa K, Baba N, Aizawa S-I. 1996. *J. Mol. Biol.* 255:458–75

31. Suzuki H, Yonekura K, Murata K, Hirai T, Oosawa K, Namba K. 1998. *J. Struct. Biol.* 124:104–14

32. Yamaguchi S, Aizawa S-I, Kihara M, Isomura M, Jones CJ, Macnab RM. 1986. *J. Bacteriol.* 168:1172–79

33. Yamaguchi S, Fujita H, Ishihara A, Aizawa S-I, Macnab RM. 1986. *J. Bacteriol.* 166:187–93

34. Welch M, Oosawa K, Aizawa S-I, Eisenbach M. 1993. *Proc. Natl. Acad. Sci. USA* 90:8787–91

35. Welch M, Oosawa K, Aizawa S-I, Eisenbach M. 1994. *Biochemistry* 33:10470–76

36. Toker AS, Macnab RM. 1997. *J. Mol. Biol.* 273:623–34

37. Bren A, Eisenbach M. 1998. *J. Mol. Biol.* 278:507–14

38. Oosawa K, Ueno T, Aizawa S-I. 1994. *J. Bacteriol.* 176:3683–91

39. Marykwas DL, Schmidt SA, Berg HC. 1996. *J. Mol. Biol.* 256:564–76

40. Tang H, Braun TF, Blair DF. 1996. *J. Mol. Biol.* 261:209–21

41. Francis NR, Irikura VM, Yamaguchi S, DeRosier DJ, Macnab RM. 1992. *Proc. Natl. Acad. Sci. USA* 89:6304–8

42. Thomas DR, Morgan DG, DeRosier DJ. 2001. *J. Bacteriol.* 183:6404–12

43. Kihara M, Francis NR, DeRosier DJ, Macnab RM. 1996. *J. Bacteriol.* 178:4582–89

44. Macnab RM. 1995. In *Two-Component Signal Transduction*, ed. JA Hoch, TJ

Silhavy, pp. 181–99. Washington, DC: Am. Soc. Microbiol.

45. Zhao R, Schuster SC, Khan S. 1995. *J. Mol. Biol.* 251:400–12

46. Zhao R, Pathak N, Jaffe H, Reese TS, Khan S. 1996. *J. Mol. Biol.* 261:195–208

47. Lloyd SA, Tang H, Wang X, Billings S, Blair DF. 1996. *J. Bacteriol.* 178:223–31

48. Thomas DR, Morgan DG, DeRosier DJ. 1999. *Proc. Natl. Acad. Sci. USA* 96:10134–39

49. Ridgway HF, Silverman M, Simon MI. 1977. *J. Bacteriol.* 132:657–65

50. Coulton JW, Murray RGE. 1978. *J. Bacteriol.* 136:1047–49

51. Khan S, Dapice M, Reese TS. 1988. *J. Mol. Biol.* 202:575–84

52. Khan S, Khan IH, Reese TS. 1991. *J. Bacteriol.* 173:2888–96

53. Khan S, Ivey DM, Krulwich TA. 1992. *J. Bacteriol.* 174:5123–26

54. Dean GE, Macnab RM, Stader J, Matsumura P, Burke C. 1984. *J. Bacteriol.* 159:991–99

55. Blair DF, Berg HC. 1991. *J. Mol. Biol.* 221:1433–42

56. Zhou J, Fazzio RT, Blair DF. 1995. *J. Mol. Biol.* 251:237–42

57. Stader J, Matsumura P, Vacante D, Dean GE, Macnab RM. 1986. *J. Bacteriol.* 166:244–52

58. Chun SY, Parkinson JS. 1988. *Science* 239:276–78

59. De Mot R, Vanderleyden J. 1994. *Mol. Microbiol.* 12:333–34

60. Sato K, Homma M. 2000. *J. Biol. Chem.* 275:5718–22

61. Braun TF, Blair DF. 2001. *Biochemistry* 40:13051–59

62. Sharp LL, Zhou J, Blair DF. 1995. *Biochemistry* 34:9166–71

63. Sharp LL, Zhou J, Blair DF. 1995. *Proc. Natl. Acad. Sci. USA* 92:7946–50

64. Garza AG, Bronstein PA, Valdez PA, Harris-Haller LW, Manson MD. 1996. *J. Bacteriol.* 178:6116–22

65. Garza AG, Harris-Haller LW, Stoebner RA, Manson MD. 1995. *Proc. Natl. Acad. Sci. USA* 92:1970–74

66. Garza AG, Biran R, Wohlschlegel JA, Manson MD. 1996. *J. Mol. Biol.* 258:270–85

67. Zhou J, Blair DF. 1997. *J. Mol. Biol.* 273:428–39

68. Lloyd SA, Blair DF. 1997. *J. Mol. Biol.* 266:733–44

69. Zhou J, Lloyd SA, Blair DF. 1998. *Proc. Natl. Acad. Sci. USA* 95:6436–41

70. Zhou J, Sharp LL, Tang HL, Lloyd SA, Billings S, et al. 1998. *J. Bacteriol.* 180:2729–35

71. Braun TF, Poulson S, Gully JB, Empey JC, Van Way S, et al. 1999. *J. Bacteriol.* 181:3542–51

72. Kojima S, Blair DF. 2001. *Biochemistry* 40:13041–50

73. Lloyd SA, Whitby FG, Blair DF, Hill CP. 1999. *Nature* 400:472–75

74. Brown PN, Hill CP, Blair DF. 2002. *EMBO J.* 21:3225–34

75. Komeda Y. 1982. *J. Bacteriol.* 150:16–26

76. Kutsukake K, Ohya Y, Iino T. 1990. *J. Bacteriol.* 172:741–47

77. Liu X, Matsumura P. 1994. *J. Bacteriol.* 176:7345–51

78. Adler J, Templeton B. 1967. *J. Gen. Microbiol.* 46:175–84

79. Komeda Y, Suzuki H, Ishidsu J-I, Iino T. 1975. *Mol. Gen. Genet.* 142:289–98

80. Bertin P, Terao E, Lee EH, Lejeune P, Colson C, et al. 1994. *J. Bacteriol.* 176:5537–40

81. Kutsukake K. 1997. *Mol. Gen. Genet.* 254:440–48

82. Shi W, Zhou Y, Wild J, Adler J, Gross CA. 1992. *J. Bacteriol.* 174:6256–63

83. Pruss BM, Matsumura P. 1997. *J. Bacteriol.* 179:5602–4

84. Clegg S, Hughes KT. 2002. *J. Bacteriol.* 184:1209–13

85. Aizawa S-I, Kubori T. 1998. *Genes Cells* 3:625–34

86. Harshey RM. 1994. *Mol. Microbiol.* 13:389–94

87. Harshey RM, Matsuyama T. 1994. *Proc. Natl. Acad. Sci. USA* 91:8631–35

88. Burkart M, Toguchi A, Harshey RM. 1998. *Proc. Natl. Acad. Sci. USA* 95:2568–73

89. Ohnishi K, Kutsukake K, Suzuki H, Iino T. 1990. *Mol. Gen. Genet.* 221:139–47

90. Gillen KL, Hughes KT. 1991. *J. Bacteriol.* 173:2301–10

91. Gillen KL, Hughes KT. 1991. *J. Bacteriol.* 173:6453–59

92. Ohnishi K, Kutsukake K, Suzuki H, Iino T. 1992. *Mol. Microbiol.* 6:3149–57

93. Gillen KL, Hughes KT. 1993. *J. Bacteriol.* 175:7006–15

94. Kutsukake K. 1994. *Mol. Gen. Genet.* 243:605–12

95. Hughes KT, Gillen KL, Semon MJ, Karlinsey JE. 1993. *Science* 262:1277–80

96. Daughdrill GW, Chadsey MS, Karlinsey JE, Hughes KT, Dahlquist FW. 1997. *Nat. Struct. Biol.* 4:285–91

97. Homma M, Kutsukake K, Iino T, Yamaguchi S. 1984. *J. Bacteriol.* 157: 100–8

98. Kutsukake K, Ide N. 1995. *Mol. Gen. Genet.* 247:275–81

99. Karlinsey JE, Tanaka S, Bettenworth V, Yamaguchi S, Boos W, et al. 2000. *Mol. Microbiol.* 37:1220–31

100. Kalir S, McClure J, Pabbaraju K, Southward C, Ronen M, et al. 2001. *Science* 292:2080–83

101. Aizawa S-I. 1996. *Mol. Microbiol.* 19:1–5

102. Macnab RM. 1999. *J. Bacteriol.* 181: 7149–53

103. Suzuki T, Iino T, Horiguchi T, Yamaguchi S. 1978. *J. Bacteriol.* 133:904–15

104. Suzuki T, Komeda Y. 1981. *J. Bacteriol.* 145:1036–41

105. Kubori T, Shimamoto N, Yamaguchi S, Namba K, Aizawa S-I. 1992. *J. Mol. Biol.* 226:433–46

106. Kubori T, Yamaguchi S, Aizawa S-I. 1997. *J. Bacteriol.* 179:813–17

107. Vogler AP, Homma M, Irikura VM, Macnab RM. 1991. *J. Bacteriol.* 173: 3564–72

108. Malakooti J, Ely B, Matsumura P. 1994. *J. Bacteriol.* 176:189–97

109. Fan F, Ohnishi K, Francis NR, Macnab RM. 1997. *Mol. Microbiol.* 26:1035–46

110. Ohnishi K, Fan F, Schoenhals GJ, Kihara M, Macnab RM. 1997. *J. Bacteriol.* 179: 6092–99

111. Minamino T, Macnab RM. 1999. *J. Bacteriol.* 181:1388–94

112. Minamino T, Macnab RM. 2000. *J. Bacteriol.* 182:4906–14

113. Kihara M, Minamino T, Yamaguchi S, Macnab RM. 2001. *J. Bacteriol.* 183: 1655–62

114. Dreyfus G, Williams AW, Kawagishi I, Macnab RM. 1993. *J. Bacteriol.* 175: 3131–38

115. Fan F, Macnab RM. 1996. *J. Biol. Chem.* 271:31981–88

116. Minamino T, Macnab RM. 2000. *Mol. Microbiol.* 37:1494–503

117. Kubori T, Matsushima Y, Nakamura D, Uralil J, Lara-Tejero M, et al. 1998. *Science* 280:602–5

118. Kubori T, Sukhan A, Aizawa S-I, Galán JE. 2000. *Proc. Natl. Acad. Sci. USA* 97:10225–30

119. Hueck CJ. 1998. *Microbiol. Mol. Biol. Rev.* 62:379–433

120. Yokoseki T, Kutsukake K, Ohnishi K, Iino T. 1995. *Microbiology* 141:1715–22

121. Fraser GM, Bennett JCQ, Hughes C. 1999. *Mol. Microbiol.* 32:569–80

122. Minamino T, Macnab RM. 2000. *Mol. Microbiol.* 35:1052–64

123. Minamino T, Chu R, Yamaguchi S, Macnab RM. 2000. *J. Bacteriol.* 182: 4207–15

124. Bennett JCQ, Thomas J, Fraser GM, Hughes C. 2001. *Mol. Microbiol.* 39:781–91

125. Auvray F, Thomas J, Fraser GM, Hughes C. 2001. *J. Mol. Biol.* 308:221–29

126. Bennett JCQ, Hughes C. 2000. *Trends Microbiol.* 8:202–4

127. Karlinsey JE, Lonner J, Brown KL, Hughes KT. 2000. *Cell* 102:487–97

128. Homma M, Kutsukake K, Hasebe M, Iino T, Macnab RM. 1990. *J. Mol. Biol.* 211:465–77

129. Müller V, Jones CJ, Kawagishi I, Aizawa S-I, Macnab RM. 1992. *J. Bacteriol.* 174:2298–304

130. Minamino T, Yamaguchi S, Macnab RM. 2000. *J. Bacteriol.* 182:3029–36

131. Homma M, Komeda Y, Iino T, Macnab RM. 1987. *J. Bacteriol.* 169:1493–98

132. Jones CJ, Homma M, Macnab RM. 1989. *J. Bacteriol.* 171:3890–900

133. Nambu T, Kutsukake K. 2000. *Microbiology* 146:1171–78

134. Dailey FE, Berg HC. 1993. *Proc. Natl. Acad. Sci. USA* 90:1043–47

135. Hirano T, Minamino T, Macnab RM. 2001. *J. Mol. Biol.* 312:359–69

136. Schoenhals GJ, Macnab RM. 1996. *J. Bacteriol.* 178:4200–7

137. Ohnishi K, Ohto Y, Aizawa S-I, Macnab RM, Iino T. 1994. *J. Bacteriol.* 176:2272–81

138. Hirano T, Yamaguchi S, Oosawa K, Aizawa S-I. 1994. *J. Bacteriol.* 176:5439–49

139. Silverman M, Simon M. 1972. *J. Bacteriol.* 112:986–93

140. Patterson-Delafield J, Martinez RJ, Stocker BAD, Yamaguchi S. 1973. *Arch. Microbiol.* 90:107–20

141. Koroyasu S, Yamazato M, Hirano T, Aizawa S-I. 1998. *Biophys. J.* 74:436–43

142. Williams AW, Yamaguchi S, Togashi F, Aizawa S-I, Kawagishi I, Macnab RM. 1996. *J. Bacteriol.* 178:2960–70

143. Minamino T, González-Pedrajo B, Yamaguchi K, Aizawa S-I, Macnab RM. 1999. *Mol. Microbiol.* 34:295–304

144. Muramoto K, Makishima S, Aizawa S-I, Macnab RM. 1999. *J. Bacteriol.* 181:5808–13

145. Kutsukake K, Minamino T, Yokoseki T. 1994. *J. Bacteriol.* 176:7625–29

146. Makishima S, Komoriya K, Yamaguchi S, Aizawa S-I. 2001. *Science* 291:2411–13

147. Ikeda T, Homma M, Iino T, Asakura S, Kamiya R. 1987. *J. Bacteriol.* 169:1168–73

148. Iino T. 1969. *J. Gen. Microbiol.* 56:227–39

149. Emerson SU, Tokuyasu K, Simon MI. 1970. *Science* 169:190–92

150. Homma M, Fujita H, Yamaguchi S, Iino T. 1984. *J. Bacteriol.* 159:1056–59

151. Kagawa H, Morisawa H, Enomoto M. 1981. *J. Mol. Biol.* 153:465–70

152. Kagawa H, Nishiyama T, Yamaguchi S. 1983. *J. Bacteriol.* 155:435–37

153. Ikeda T, Yamaguchi S, Hotani H. 1993. *J. Biochem.* 114:39–44

154. Ikeda T, Oosawa K, Hotani H. 1996. *J. Mol. Biol.* 259:679–86

155. Yonekura K, Maki S, Morgan DG, DeRosier DJ, Vonderviszt F, et al. 2000. *Science* 290:2148–52

156. Iino T. 1974. *J. Supramol. Struct.* 2:372–84

157. Yonekura K, Maki-Yonekura S, Namba K. 2002. *Res. Microbiol.* 153:191–97

158. Stolz B, Berg HC. 1991. *J. Bacteriol.* 173:7033–37

159. Van Way S, Hosking ER, Braun TF, Manson MD. 2000. *J. Mol. Biol.* 297:7–24

160. Larsen SH, Adler J, Gargus JJ, Hogg RW. 1974. *Proc. Natl. Acad. Sci. USA* 71:1239–43

161. Khan S, Macnab RM. 1980. *J. Mol. Biol.* 138:563–97

162. Khan S, Macnab RM. 1980. *J. Mol. Biol.* 138:599–614

163. Ravid S, Eisenbach M. 1984. *J. Bacteriol.* 158:1208–10

164. Harold FM, Maloney PC. 1996. See Ref. 261, pp. 283–306

165. Fung DC, Berg HC. 1995. *Nature* 375:809–12

166. Meister M, Berg HC. 1987. *Biophys. J.* 52:413–19

167. Khan S, Dapice M, Humayun I. 1990. *Biophys. J.* 57:779–96

168. Chen X, Berg HC. 2000. *Biophys. J.* 78:2280–84

169. Shioi J-I, Matsuura S, Imae Y. 1980. *J. Bacteriol.* 144:891–97

170. van der Drift C, Duiverman J, Bexkens H, Krijnen A. 1975. *J. Bacteriol.* 124:1142–47

171. Manson MD, Tedesco P, Berg HC, Harold FM, van der Drift C. 1977. *Proc. Natl. Acad. Sci. USA* 74:3060–64

172. Manson MD, Tedesco PM, Berg HC. 1980. *J. Mol. Biol.* 138:541–61

173. Lowe G, Meister M, Berg HC. 1987. *Nature* 325:637–40

174. Berg HC, Anderson RA. 1973. *Nature* 245:380–82

175. Meister M, Lowe G, Berg HC. 1987. *Cell* 49:643–50

176. Weibull C. 1953. *J. Bacteriol.* 66:688–95

177. Imae Y, Atsumi T. 1989. *J. Bioenerg. Biomembr.* 21:705–16

178. Imae Y. 1991. In *New Era of Bioenergetics*, ed. Y Mukohata, pp. 197–221. Tokyo: Academic

179. Asai Y, Kojima S, Kato H, Nishioka N, Kawagishi I, Homma M. 1997. *J. Bacteriol.* 179:5104–10

180. Magariyama Y, Sugiyama S, Muramoto K, Maekawa Y, Kawagishi I, et al. 1994. *Nature* 371:752

181. Muramoto K, Kawagishi I, Kudo S, Magariyama Y, Imae Y, Homma M. 1995. *J. Mol. Biol.* 251:50–58

182. Sugiyama S, Cragoe EJ Jr, Imae Y. 1988. *J. Biol. Chem.* 263:8215–19

183. Atsumi T, Sugiyama S, Cragoe EJ Jr, Imae Y. 1990. *J. Bacteriol.* 172:1634–39

184. Kojima S, Atsumi T, Muramoto K, Kudo S, Kawagishi I, Homma M. 1997. *J. Mol. Biol.* 265:310–18

185. Kojima S, Asai Y, Atsumi T, Kawagishi I, Homma M. 1999. *J. Mol. Biol.* 285:1537–47

186. Asai Y, Kawagishi I, Sockett RE, Homma M. 1999. *J. Bacteriol.* 181:6332–38

187. Asai Y, Kawagishi I, Sockett RE, Homma M. 2000. *EMBO J.* 19:3639–48

188. Stocker BAD, Zinder ND, Lederberg J. 1953. *J. Gen. Microbiol.* 9:410–33

189. Silverman M, Matsumura P, Simon M. 1976. *Proc. Natl. Acad. Sci. USA* 73:3126–30

190. Block SM, Berg HC. 1984. *Nature* 309:470–72

191. Silverman M, Simon M. 1974. *Nature* 249:73–74

192. Blair DF, Berg HC. 1988. *Science* 242:1678–81

193. Berg HC. 1976. In *Cell Motility, Cold Spring Harbor Conferences on Cell Proliferation*, ed. R Goldman, T Pollard, J Rosenbaum, pp. 47–56. Cold Spring Harbor, NY: Cold Spring Harbor Lab.

194. Block SM, Blair DF, Berg HC. 1989. *Nature* 338:514–17

195. Block SM, Blair DF, Berg HC. 1991. *Cytometry* 12:492–96

196. Cox DR, Lewis PAW. 1966. *The Statistical Analysis of Series of Events*. London: Methuen. 285 pp.

197. Samuel ADT, Berg HC. 1995. *Proc. Natl. Acad. Sci. USA* 92:3502–6

198. Berg HC, Manson MD, Conley MP. 1982. *Symp. Soc. Exp. Biol.* 35:1–31

199. Samuel ADT, Berg HC. 1996. *Biophys. J.* 71:918–23

200. Svoboda K, Mitra PP, Block SM. 1994. *Proc. Natl. Acad. Sci. USA* 91:11782–86

201. Kara-Ivanov M, Eisenbach M, Caplan SR. 1995. *Biophys. J.* 69:250–63

202. Berg HC, Turner L. 1993. *Biophys. J.* 65:2201–16

203. Chen X, Berg HC. 2000. *Biophys. J.* 78:1036–41

204. Berry RM, Berg HC. 1997. *Proc. Natl. Acad. Sci. USA* 94:14433–37

205. Berg HC, Turner L. 1979. *Nature* 278:349–51

206. Garcia de la Torre J, Bloomfield VA. 1981. *Q. Rev. Biophys.* 14:81–139

207. Jeffery GB. 1915. *Proc. London Math. Soc.* 14:327–38

208. Washizu M, Kurahashi Y, Iochi H, Kurosawa O, Aizawa S-I, et al. 1993. *IEEE Trans. Ind. Appl.* 29:286–94

209. Okino H, Isomura M, Yamaguchi S, Magariyama Y, Kudo S, Aizawa S-I. 1989. *J. Bacteriol.* 171:2075–82

210. Berry RM, Berg HC. 1999. *Biophys. J.* 76:580–87

211. Berg HC. 2000. *Philos. Trans. R. Soc. London Ser. B* 355:491–501

212. Khan S, Berg HC. 1983. *Cell* 32:913–19

213. Blair DF, Berg HC. 1990. *Cell* 60:439–49

214. Khan S, Meister M, Berg HC. 1985. *J. Mol. Biol.* 184:645–56

215. Ryu WS, Berry RM, Berg HC. 2000. *Nature* 403:444–47

216. Block SM, Segall JE, Berg HC. 1983. *J. Bacteriol.* 154:312–23

217. Kuo SC, Koshland DE Jr. 1989. *J. Bacteriol.* 171:6279–87

218. Eisenbach M, Wolf A, Welch M, Caplan SR, Lapidus IR, et al. 1990. *J. Mol. Biol.* 211:551–63

219. Armstrong JB, Adler J, Dahl MM. 1967. *J. Bacteriol.* 93:390–98

220. Berg HC, Block SM, Conley MP, Nathan AR, Power JN, Wolfe AJ. 1987. *Rev. Sci. Instrum.* 58:418–23

221. Kudo S, Magariyama Y, Aizawa S-I. 1990. *Nature* 346:677–80

222. Meister M, Caplan SR, Berg HC. 1989. *Biophys. J.* 55:905–14

223. Turner L, Caplan SR, Berg HC. 1996. *Biophys. J.* 71:2227–33

224. Prasad K, Caplan SR, Eisenbach M. 1998. *J. Mol. Biol.* 280:821–28

225. Scharf BE, Fahrner KA, Turner L, Berg HC. 1998. *Proc. Natl. Acad. Sci. USA* 95:201–6

226. Alon U, Camarena L, Surette MG, Aguera y Arcas B, Liu Y, et al. 1998. *EMBO J.* 17:4238–48

227. Monod J, Wyman J, Changeux J-P. 1965. *J. Mol. Biol.* 12:88–118

228. Turner L, Samuel ADT, Stern AS, Berg HC. 1999. *Biophys. J.* 77:597–603

229. Cluzel P, Surette M, Leibler S. 2000. *Science* 287:1652–55

230. Sourjik V, Berg HC. 2002. *Proc. Natl. Acad. Sci. USA.* 99:12669–74

231. Khan S, Pierce D, Vale RD. 2000. *Curr. Biol.* 10:927–30

232. Duke TAJ, Le Novère N, Bray D. 2001. *J. Mol. Biol.* 308:541–53

233. Ludwig W. 1930. *Z. Vergl. Physiol.* 13:397–504

234. Taylor GI. 1952. *Proc. R. Soc. London Ser. A* 211:225–39

235. Purcell EM. 1977. *Am. J. Phys.* 45:3–11

236. Berg HC. 1996. *Proc. Natl. Acad. Sci. USA* 93:14225–28

237. Howard J. 2001. *Mechanics of Motor Proteins and the Cytoskeleton.* Sunderland, MA: Sinauer

238. Iwazawa J, Imae Y, Kobayasi S. 1993. *Biophys. J.* 64:925–33

239. Berg HC, Khan S. 1983. In *Mobility and Recognition in Cell Biology*, ed. H Sund, C Veeger, pp. 485–97. Berlin: de Gruyter

240. Elston TC, Oster G. 1997. *Biophys. J.* 73:703–21

241. Läuger P. 1988. *Biophys. J.* 53:53–65

242. Berg HC. 2003. In *The Enzymes,* Vol. XXIII, *Energy Coupling and Molecular Motors.* New York: Academic. In press

243. Läuger P, Kleutsch B. 1990. *Comments Theor. Biol.* 2:99–123

244. Caplan SR, Kara-Ivanov M. 1993. *Int. Rev. Cytol.* 147:97–164

245. Schuster SC, Khan S. 1994. *Annu. Rev. Biophys. Biomol. Struct.* 23:509–39

246. Macnab RM. 1996. See Ref. 261, pp. 123–45

247. Khan S. 1997. *Biochim. Biophys. Acta* 1322:86–105

248. Berry RB, Armitage JP. 1999. *Adv. Microb. Physiol.* 41:291–337

249. Berry RB. 2000. *Philos. Trans. R. Soc. London Ser. B* 355:503–9

250. Berg HC. 2000. *Phys. Today* 53:24–29

251. Walz D, Caplan SR. 2002. *Bioelectrochemistry* 55:89–92

252. McCarter LL. 2001. *Microbiol. Mol. Biol. Rev.* 65:445–62

253. Yorimitsu T, Homma M. 2001. *Biochim. Biophys. Acta* 1505:82–93

254. Macnab RM. 1992. *Annu. Rev. Genet.* 26:131–58

255. Chilcott GS, Hughes KT. 2000. *Microbiol. Mol. Biol. Rev.* 64:694–708

256. Aldridge P, Hughes KT. 2002. *Curr. Opin. Microbiol.* 5:160–65

257. Bustamante C, Keller D, Oster G. 2001. *Acc. Chem. Res.* 34:412–20

258. Iino T. 1985. In *Sensing and Response in Microorganisms*, ed. M Eisenbach, M Balaban, pp. 83–92. Amsterdam: Elsevier

259. Macnab RM. 1976. *J. Clin. Microbiol.* 4:258–65

260. Block SM, Fahrner K, Berg HC. 1991. *J. Bacteriol.* 173:933–36

261. Neidhardt FC, Curtiss R, Ingraham JL, Lin ECC, Low KB, et al., eds. 1996. *Escherichia coli and Salmonella: Cellular and Molecular Biology.* Washington, DC: Am. Soc. Microbiol.

CONTENTS